



CERN-EP-2023-268
20 November 2023

Measurements of chemical potentials in Pb–Pb collisions at $\sqrt{s_{NN}} = 5.02 \text{ TeV}$

ALICE Collaboration*

Abstract

This Letter presents the most precise measurement to date of the matter–antimatter imbalance at midrapidity in Pb–Pb collisions at a center-of-mass energy per nucleon pair $\sqrt{s_{NN}} = 5.02 \text{ TeV}$. Using the Statistical Hadronization framework, it is possible to obtain the value of the electric charge and baryon chemical potentials, $\mu_Q = -0.18 \pm 0.90 \text{ MeV}$ and $\mu_B = 0.71 \pm 0.45 \text{ MeV}$, with unprecedented precision. A centrality-differential study of the antiparticle-to-particle yield ratios of charged pions, protons, Ω -baryons, and light (hyper)nuclei is performed. These results indicate that the system created in Pb–Pb collisions at the LHC is on average baryon-free and electrically neutral at midrapidity.

arXiv:2311.13332v3 [nucl-ex] 1 Oct 2024

Introduction. Nuclear matter at extremely high energy densities can be generated in the laboratory through relativistic heavy-ion collisions [1–3]. At the LHC, the beam remnants from the collision are located at rapidities $y \approx \pm 6$ and a fraction of the collision energy is deposited at midrapidity [4]. In this region, particles are formed from a nearly baryon number and electric charge free medium. This process can be described in the Color Glass Condensate model via gluon radiation by static quarks, frozen by time dilation [5]. Conversely, string-fragmentation models explain it through the breaking of color flux tubes. Part of the initial baryon number can be transported to midrapidity via either baryon junction formation [6] or diquark breaking [7]. This phenomenon, known as nuclear stopping, influences the net-baryon density of the system formed at midrapidity [8–10]. The baryon number transport is minimal at the LHC, and the nuclear transparency regime [11] is reached. In this regime, conditions akin to those of the early Universe are replicated, where nearly equal abundances of matter and antimatter were present, as described by the standard cosmological model [12]. Experimentally, one can gauge the extent to which heavy-ion collisions approach the early Universe conditions by measuring the antimatter-to-matter yield ratios across various hadron species.

A comprehensive framework for interpreting these ratios is provided by the Statistical Hadronization Model (SHM)[13–18]. Among the several models that can be used to describe a heavy-ion collision, the SHM is the most successful in describing the yields of all light-flavor hadronic species, which are determined starting from the partition function of the fireball at the freeze-out of inelastic scatterings. This fireball is an equilibrated gas composed of hadrons and resonances. Because of the substantial particle multiplicity and the finite kinematical acceptance, a Grand Canonical (GC) ensemble description is employed for heavy-ion collisions. In this approach, the conservation of charges, namely the baryon number (B), the electric charge (Q), and strangeness (S), is regulated by the corresponding chemical potentials μ_B , μ_Q , and μ_S , respectively [19, 20]. The baryon chemical potential μ_B represents the net-baryon density of the system, with $\mu_B = 0$ corresponding to an equilibrated gas composed of hadrons and resonances with same amount of baryons and antibaryons. The electric charge potential μ_Q encodes the positive-negative charge imbalance of the gas; it is connected to μ_B by the atomic-to-mass-number ratio Z/A of the colliding ions [21, 22]. The requirement of strangeness neutrality constrains μ_S throughout the entire volume of the fireball [21, 22]. Chemical potentials determine the abundance of hadrons through the fugacity, $\lambda_i = \exp[(B_i\mu_B + Q_i\mu_Q + S_i\mu_S)/T_{\text{ch}}]$, where B_i , Q_i , and S_i denote the quantum numbers of the considered species i , and T_{ch} is the chemical freeze-out temperature, at which hadron yields are determined.

Over the last three decades, the asymmetry between antimatter and matter of the fireball has been systematically studied at different experimental facilities [23–38]. The decreasing trend of μ_B , from about 400 MeV at the SPS to 20 MeV at the top RHIC energy of 200 GeV, and $\mu_B = 0.7 \pm 3.8$ MeV at the LHC is consistent with the decrease of baryon number transport to midrapidity with increasing beam rapidity [36, 37, 39–79]. The formation of baryon number free matter at midrapidity was first reported in pp collisions by ALICE, which observed that the \bar{p}/p yield ratio is compatible with unity [80]. At fixed collision energy, it is also possible to explore nuclear transparency as a function of centrality, i.e., the transverse displacement between the centers of the colliding nuclei, as it affects the dynamics of the colliding nucleons. In particular, a slight increase in μ_B from peripheral to central (head-on) collisions was observed at low energies by STAR at the RHIC beam energy scan [79]. These results were obtained by either comparing the SHM predictions with the measured yields of hadrons and their antimatter counterparts [81] or by directly fitting antiparticle-to-particle yield ratios [76, 79].

In this Letter, we report the most precise estimation to date of μ_B and μ_Q obtained from a set of antiparticle-to-particle yield ratios. Compared to previous estimations, the precision of the current results has improved by about an order of magnitude. This improvement in precision is attributed to the proper treatment of the cancelation of particle-antiparticle correlated uncertainties and the reduced dependence on model parameters, such as the system volume, V , which is eliminated in the antiparticle-to-particle

yield ratios. The analyzed species are charged pions, protons, Ω^- baryons, and light (hyper)nuclei. (Anti)protons are the most abundantly produced (anti)baryons at midrapidity (≈ 35 and ≈ 2 protons on average in central and peripheral Pb–Pb collisions, respectively [82]). Consequently, the antiproton-to-proton yield ratio can probe the antibaryon-to-baryon imbalance [80, 83] with high precision. On the other hand, the sensitivity to baryon asymmetry is enhanced when light (hyper)nuclei are included because of their larger baryon content. In this work, ${}^3\text{He}$, its isobar ${}^3\text{H}$, and hypertriton ${}^3_{\Lambda}\text{H}$, which is a bound state of a proton, a neutron, and a Λ , along with their antimatter counterparts, are considered¹. The ratio of oppositely charged pions provides a precise constraint on the imbalance of electric charge, as the yield ratio depends predominantly on μ_Q . Finally, the dependence of antimatter-to-matter ratios on strangeness is probed with (anti) Ω^- baryons, which, unlike (anti) Λ and (anti) Ξ^- , have negligible contamination coming from heavier hadron decays.

The ALICE detector and data analysis. The results reported in this analysis are obtained from a sample of Pb–Pb collisions at $\sqrt{s_{\text{NN}}} = 5.02$ TeV collected in 2018 by ALICE at the LHC. The ALICE apparatus and its performance are described in detail in Refs. [85, 86]. The minimum-bias collision and centrality triggers are provided by the V0 system [87], which is composed of two arrays of plastic scintillators covering the forward ($2.8 < \eta < 5.1$) and backward ($-3.7 < \eta < -1.7$) regions of pseudorapidity. The coincidence of signals in both detectors determines the minimum bias trigger. The amplitude of the V0 signal is proportional to the charge deposited in the detectors, which is related to the produced charged-particle multiplicity that, in turn, is controlled by the collision centrality. The V0 amplitude is then used to trigger specific categories of central and semicentral events, and to estimate centrality [88]. Five centrality intervals are considered in this Letter, namely 0–5%, 5–10%, 10–30%, 30–50%, and 50–90%, expressed as percentiles of the total hadronic cross section for Pb–Pb collisions. The position of the primary interaction vertex is required to be within a 10 cm wide region centered at the nominal interaction point to profit from the full acceptance of the ALICE central barrel detectors. Events with multiple interaction vertices are rejected to ensure the correct association of reconstructed tracks and primary vertices. The number of events passing these selections is approximately 300 million.

Charged pions, protons, ${}^3\text{He}$, and tritons produced at midrapidity, $|y| < 0.5$, are tracked in the ALICE central barrel: hereafter, charge conjugates are implied unless stated otherwise. The tracks are reconstructed within $|\eta| < 0.8$ and in the full azimuth using the Inner Tracking System (ITS) [89] and the Time Projection Chamber (TPC) [90]. These detectors are placed in a solenoid that provides a uniform magnetic field of 0.5 T parallel to the beam axis. The antiparticle-to-particle yield ratios are measured as a function of the transverse momentum p_T in the ranges $0.7 \leq p_T < 1.6$ GeV/ c for π^-/π^+ , $0.5 \leq p_T < 3$ GeV/ c for \bar{p}/p , $1.6 \leq p_T < 3$ GeV/ c for ${}^3\bar{\text{H}}/{}^3\text{H}$, and $2 \leq p_T < 8$ GeV/ c for ${}^3\bar{\text{He}}/{}^3\text{He}$ to select the bulk of the production and ensure good identification performance.

The analysis procedure for extracting particle yields is similar to the one adopted in previous analyses [82, 91, 92]. Standard selections on the χ^2 of the track fit, on the number of reconstructed track points in the ITS and the TPC, and on the distance of closest approach of the extrapolation of the track to the primary interaction vertex ensure a good reconstruction of tracks originating from the collisions. Particle identification is performed on a statistical basis by measuring the specific energy loss (dE/dx) in both the TPC and the ITS, and particle velocity depending on the transverse momentum of the measured particles with the Time-Of-Flight detector (TOF). Further details about the particle identification are provided in Appendix A.1.

The residual contamination due to hyperon weak decays and spallation reactions of primary particles in the apparatus is evaluated by fitting the measured distance of closest approach distribution in the plane transverse to the beam axis with templates computed via Monte Carlo (MC) simulations for the various processes involved [82, 91, 92]. The extracted yields are corrected for the detector acceptance and

¹(Anti)deuterons, $d(\bar{d})$ are not considered in this Letter since the efficiency correction for \bar{d} is based on the \bar{d} absorption cross section extracted by the ALICE Collaboration from the measured \bar{d}/d yield ratio itself [84].

candidate selection efficiency, computed using MC simulations, as the fraction of particles reconstructed out of all MC-generated primary particles. The Pb–Pb event is generated with HIJING [93], while the particles are transported through a realistic model of the ALICE apparatus with GEANT4 [94]. To increase the simulated sample size protons, ^3He nuclei, and tritons are injected on top of each HIJING event. The available measurements of hadron inelastic cross sections are used to correct the GEANT4 parameterizations of the corresponding reactions [95–109].

The $^3_\Lambda\text{H}$ candidates are reconstructed from their two-body charged mesonic decay $^3_\Lambda\text{H} \rightarrow ^3\text{He} + \pi^-$. The reconstruction algorithm is the same as the one applied in previous measurements [110–113]. The Ω^- is reconstructed with a similar procedure from the decay into a charged kaon and a Λ baryon, that, in turn, is reconstructed from its charged two-body decay, $\Omega^- \rightarrow \text{K}^- + \Lambda (\rightarrow \pi^- + \text{p})$ [114–116]. The ratios are extracted in intervals of proper decay length $ct = cML/p$, with M , L , and p being the mass, trajectory length, and candidate momentum, respectively. In particular, $2 \leq ct < 35$ cm for $^3_\Lambda\text{H}$ and $1 \leq ct < 10$ cm for Ω^- are used. The $^3_\Lambda\text{H}$ and Ω^- candidates are selected with Boosted Decision Tree algorithms [117], which are applied on top of preliminary kinematic and topological selections to enhance the background rejection. The Boosted Decision Tree internal parameters and selections are optimized using samples of correctly classified signal and background candidates, as explained in detail in Appendix A.2.

The invariant mass distribution of the selected candidates is fitted with a probability density function built with a Kernel Density Estimation [118, 119] in the MC for $^3_\Lambda\text{H}$, whereas an extended Crystal-Ball function is used for the Ω^- signal [120]. An exponential function is used to model the residual background in both cases. The yields extracted as the integral of the signal functions obtained from the fits are corrected by the overall selection efficiency and acceptance computed in the MC simulations. As in previous $^3_\Lambda\text{H}$ analyses [113], an absorption correction factor is included to account for undetected candidates absorbed in the detector material before their decay.

The following systematic uncertainty contributions are estimated for the antiparticle-to-particle yield ratios: candidate selection and signal extraction, MC data sample size, material budget uncertainty, absorption cross section uncertainties, and magnetic field polarity. The details about the estimation and values of such contributions are reported in Appendix A.4.

Results. The fully corrected antiparticle-to-particle yield ratios do not exhibit any significant dependence on p_T and ct (see Appendix A.5). This observation, which is consistent across particle species and centrality intervals, implies that the production spectra of charge-conjugate species only differ by normalization factors proportional to their yields. The antiparticle-to-particle yield ratios of each species are obtained as the averages weighted with the total uncorrelated uncertainties of the p_T - and ct -differential ratios in each centrality interval. For $^3_\Lambda\text{H}$, no statistically significant signal is observed in the 50–90% centrality range.

The chemical potentials μ_B and μ_Q are extracted by fitting the antiparticle-to-particle yield ratios with the predictions of the GC statistical hadronization model using the Thermal-FIST code [22]. The measured ratios and the SHM fit results are reported in Fig. 1. The chemical freeze-out temperature is set to $T_{\text{ch}} = 155 \pm 2$ MeV, as obtained from a fit to the ALICE data [121, 122]: its value is compatible with the pseudo-critical temperature extracted with lattice QCD calculations [123]. This value is fixed for all centralities, since in heavy-ion collisions only a mild dependence of T_{ch} on centrality is observed (less than 3% [35, 79, 121, 124]); additionally, antiparticle-to-particle yield ratios show a negligible dependence on T_{ch} for $\mu_B \approx 1$ MeV [81]. The uncertainty on T_{ch} , which is compatible with the range of variations of T_{ch} observed as a function of centrality, is considered as a centrality-correlated source of systematic uncertainty. The strangeness chemical potential μ_S is constrained in the fit from strangeness conservation. The contribution of strongly-decaying resonances is accounted in the model predictions as it cannot be directly disentangled in the data. For the χ^2 minimization, the quadratic sum of statistical and uncorrelated systematic uncertainty is considered. The effect of the centrality-correlated sources

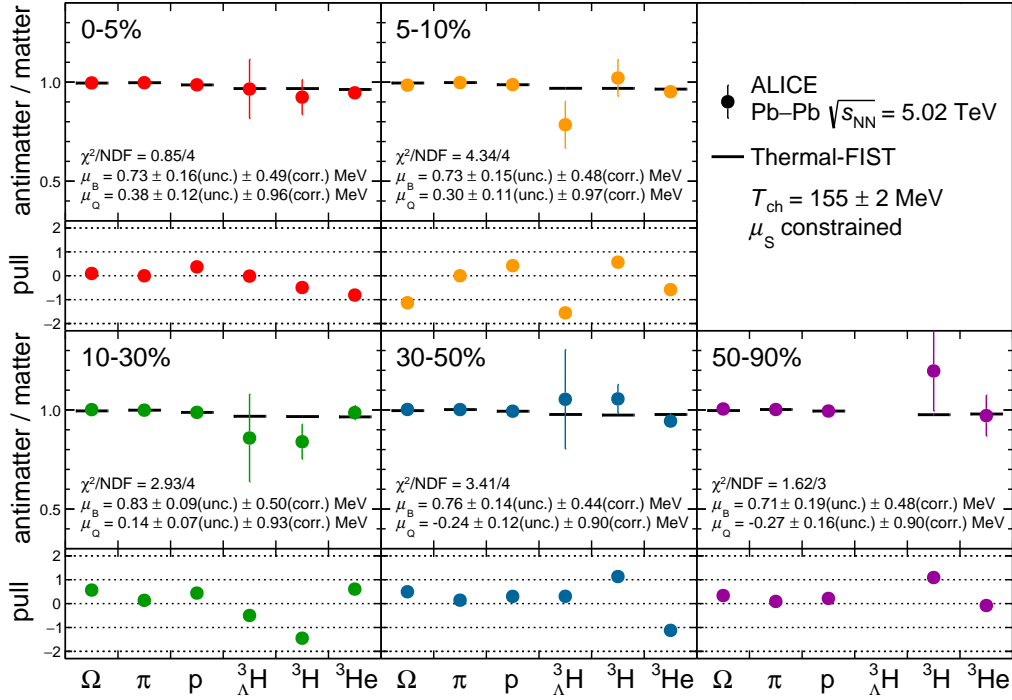


Figure 1: Upper panels: statistical hadronization model fits to the measured antiparticle-to-particle yield ratios in different centrality intervals. Error bars show the sum in quadrature of statistical and centrality-uncorrelated systematic uncertainties. When not visible, error bars are hidden by the marker. Lower panels: pull distribution, defined as the difference between data and fit values, normalized to the uncertainty in the data.

is evaluated by repeating the fit to ratios coherently increased or decreased by their uncertainties. The uncertainty assigned to μ_B and μ_Q is half of the difference between the results obtained in the two cases.

In this Letter, yield ratios are analyzed within the GC statistical model also in the most peripheral events, where canonical ensemble formulation is needed for an accurate description of hadron yields by requiring exact conservation of charges over a finite volume [125, 126]. It is known, however, that effects connected to the canonical conservation of charges cancel out when considering antiparticle-to-particle yield ratios, and their values are well described by the GC ensemble [15, 127]. Indeed, good fit quality is obtained across the 0–90% centrality range using the GC model to quantify these ratios. In addition, the yield ratio Ω^+/Ω^- is compatible with unity as expected in the SHM, where it is weakly dependent of μ_B and μ_S for $\mu_B \sim 0$ [16].

The chemical potentials obtained in different centrality intervals are shown in the left panel of Fig. 2. The contours show a negative correlation between μ_B and μ_Q , which is connected to the approximate exponential dependence of antiparticle-to-particle yield ratios on the linear combination of the chemical potentials. The centrality dependence of μ_B and μ_Q is studied by fitting independently the centrality-differential μ_B and μ_Q results with a constant function, taking into account the full correlation matrix of the measurements. Both the correlation matrices and the χ^2 profiles of the fits are reported in the Appendix. The fit probability is $P = 0.97$ for μ_B and $P = 0.64$ for μ_Q : therefore, no evidence of centrality dependence is found, even if a larger μ_B would be expected in more central collisions due to a potentially larger baryon stopping [4]. The fit of the centrality-differential values yields chemical potentials $\mu_B = 0.71 \pm 0.45$ MeV and $\mu_Q = -0.18 \pm 0.90$ MeV, which are compatible with zero within 1.6σ and 0.2σ , respectively. The comparison with the previous data point of μ_B at the LHC [35–38] shows a significant improvement in the precision by a factor larger than eight (no direct value of μ_Q was provided in that

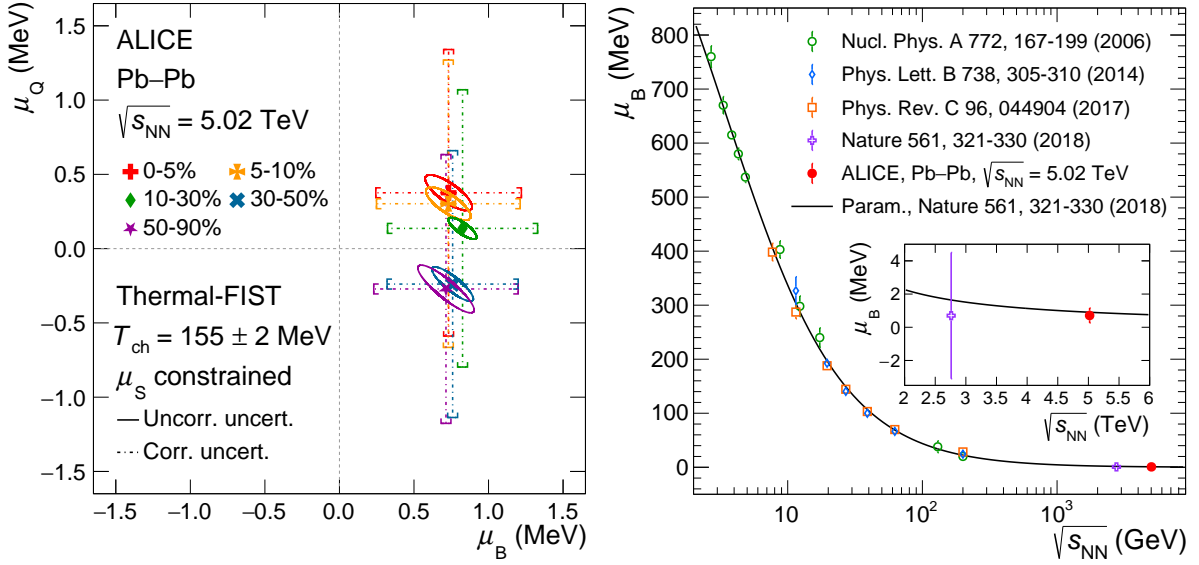


Figure 2: Left panel: μ_B and μ_Q obtained with Thermal-FIST [22] in different centrality intervals. The centrality-correlated and centrality-uncorrelated uncertainties are represented with error bars and ellipses, respectively. Right panel: μ_B extracted from data collected in Au–Au and Pb–Pb collisions at the AGS (E802, E866, E877, E895, E896, E917 Collaborations), SPS (NA44, NA49, NA47 Collaborations), RHIC (BRAHMS, PHENIX, STAR Collaboration), and LHC (ALICE Collaboration) as a function of the center-of-mass energy per nucleon–nucleon pair [76, 78, 79], and phenomenological parameterization of $\mu_B(\sqrt{s_{NN}})$ [36]. The inset shows more in detail the results obtained at the LHC [36].

study, see below). These results imply that the system created at midrapidity in Pb–Pb collisions is baryon- and electrically-neutral on average. As a consequence, this observation shows that the nuclear transparency regime is reached, i.e., baryon transport from the colliding ions to the interaction region is negligible. Because of the absence of any centrality dependence, it is also concluded that nuclear transparency is achieved even in central Pb–Pb collisions, where a larger-than-zero μ_B could be expected from a more significant baryon number transport at midrapidity.

As a cross check, the SHM fits described above are repeated by also constraining μ_Q from initial conditions via conservation laws, as it was done also in past measurements [36, 76, 79]. Specifically, the μ_Q/μ_B ratio is fixed by requiring that the average charge-to-baryon density ratio of the created hadron system, $\langle n_Q \rangle / \langle n_B \rangle$, is equivalent to the Z/A ratio of colliding nuclei, i.e., $\langle n_Q \rangle / \langle n_B \rangle = Z/A \approx 0.4$ for ^{208}Pb [21]. The μ_B values extracted from the fits in each centrality interval are successfully fitted with a constant function (fit probability $P = 0.09$). The resulting μ_B value is compatible with the one reported above within uncertainties. Similar results are obtained by fitting the antiparticle-to-particle yield ratios using the GSI-Heidelberg model [15, 37, 76], with $T_{\text{ch}} = 156.6 \pm 1.7$ MeV [38] and μ_Q is fixed to initial conditions: the average value across centrality is $\mu_B = 0.90 \pm 0.43$ MeV. The χ^2 profile of the fit is reported in Appendix C. Using the values of μ_B and μ_Q extracted in the 5% most central collisions, the inclusive net-proton density at midrapidity, $2/\langle N_{\text{part}} \rangle dN_{p-\bar{p}}/dy$, can be computed in the SHM framework. The value extracted with Thermal-FIST is $(3.4 \pm 1.4) \times 10^{-3}$, while using the GSI-Heidelberg model, a value of $5.9^{+2.2}_{-2.8} \times 10^{-3}$ is obtained. In both cases, the obtained results agree with the exponential trend as a function of beam rapidity predicted by the baryon-junction mechanism [128].

The right panel of Fig. 2 shows the comparison of the current with past estimations of μ_B as a function of the center-of-mass energy of the collision [36, 76, 78, 79]. The comparison with the previous LHC data point is highlighted in the inset of the figure. The result reported in this Letter is compatible with the extrapolation of the phenomenological parameterization based on previous data and reported in Ref. [36].

Conclusions. In summary, the most precise measurement of the asymmetry between matter and antimatter at the LHC is reported in this Letter. The asymmetry is quantified through antiparticle-to-particle yield ratios of different hadrons, which are analyzed within the statistical hadronization framework to extract the chemical potentials μ_B and μ_Q . The GC version of the model accurately describes the antiparticle-to-particle yield ratios across centrality, indicating the elimination of effects from canonical charge conservation in peripheral events. The cancelation of correlated uncertainties in these ratios leads to a significant improvement in the μ_B precision: the uncertainty on the obtained value is about one order of magnitude smaller than the previously published one [36]. In addition, a direct estimation of μ_Q is provided. Furthermore, the first centrality-differential study of chemical potentials at the LHC is reported in this Letter. The obtained chemical potentials are consistent with zero, i.e., with the nuclear transparency regime being reached across the full centrality range, thus indicating that baryon transport to midrapidity is negligible even in the most central events at the LHC.

Acknowledgements

The ALICE Collaboration would like to thank all its engineers and technicians for their invaluable contributions to the construction of the experiment and the CERN accelerator teams for the outstanding performance of the LHC complex. The ALICE Collaboration gratefully acknowledges the resources and support provided by all Grid centres and the Worldwide LHC Computing Grid (WLCG) collaboration. The ALICE Collaboration acknowledges the following funding agencies for their support in building and running the ALICE detector: A. I. Alikhanyan National Science Laboratory (Yerevan Physics Institute) Foundation (ANSL), State Committee of Science and World Federation of Scientists (WFS), Armenia; Austrian Academy of Sciences, Austrian Science Fund (FWF): [M 2467-N36] and Nationalstiftung für Forschung, Technologie und Entwicklung, Austria; Ministry of Communications and High Technologies, National Nuclear Research Center, Azerbaijan; Conselho Nacional de Desenvolvimento Científico e Tecnológico (CNPq), Financiadora de Estudos e Projetos (Finep), Fundação de Amparo à Pesquisa do Estado de São Paulo (FAPESP) and Universidade Federal do Rio Grande do Sul (UFRGS), Brazil; Bulgarian Ministry of Education and Science, within the National Roadmap for Research Infrastructures 2020-2027 (object CERN), Bulgaria; Ministry of Education of China (MOEC), Ministry of Science & Technology of China (MSTC) and National Natural Science Foundation of China (NSFC), China; Ministry of Science and Education and Croatian Science Foundation, Croatia; Centro de Aplicaciones Tecnológicas y Desarrollo Nuclear (CEADEN), Cubaenergía, Cuba; Ministry of Education, Youth and Sports of the Czech Republic, Czech Republic; The Danish Council for Independent Research | Natural Sciences, the VILLUM FONDEN and Danish National Research Foundation (DNRF), Denmark; Helsinki Institute of Physics (HIP), Finland; Commissariat à l’Energie Atomique (CEA) and Institut National de Physique Nucléaire et de Physique des Particules (IN2P3) and Centre National de la Recherche Scientifique (CNRS), France; Bundesministerium für Bildung und Forschung (BMBF) and GSI Helmholtzzentrum für Schwerionenforschung GmbH, Germany; General Secretariat for Research and Technology, Ministry of Education, Research and Religions, Greece; National Research, Development and Innovation Office, Hungary; Department of Atomic Energy Government of India (DAE), Department of Science and Technology, Government of India (DST), University Grants Commission, Government of India (UGC) and Council of Scientific and Industrial Research (CSIR), India; National Research and Innovation Agency - BRIN, Indonesia; Istituto Nazionale di Fisica Nucleare (INFN), Italy; Japanese Ministry of Education, Culture, Sports, Science and Technology (MEXT) and Japan Society for the Promotion of Science (JSPS) KAKENHI, Japan; Consejo Nacional de Ciencia (CONACYT) y Tecnología, through Fondo de Cooperación Internacional en Ciencia y Tecnología (FONCICYT) and Dirección General de Asuntos del Personal Académico (DGAPA), Mexico; Nederlandse Organisatie voor Wetenschappelijk Onderzoek (NWO), Netherlands; The Research Council of Norway, Norway; Commission on Science and Technology for Sustainable Development in the South (COMSATS), Pakistan; Pontificia Universidad Católica del Perú, Peru; Ministry of Education and Science, National Science

Centre and WUT ID-UB, Poland; Korea Institute of Science and Technology Information and National Research Foundation of Korea (NRF), Republic of Korea; Ministry of Education and Scientific Research, Institute of Atomic Physics, Ministry of Research and Innovation and Institute of Atomic Physics and Universitatea Nationala de Stiinta si Tehnologie Politehnica Bucuresti, Romania; Ministry of Education, Science, Research and Sport of the Slovak Republic, Slovakia; National Research Foundation of South Africa, South Africa; Swedish Research Council (VR) and Knut & Alice Wallenberg Foundation (KAW), Sweden; European Organization for Nuclear Research, Switzerland; Suranaree University of Technology (SUT), National Science and Technology Development Agency (NSTDA) and National Science, Research and Innovation Fund (NSRF via PMU-B B05F650021), Thailand; Turkish Energy, Nuclear and Mineral Research Agency (TENMAK), Turkey; National Academy of Sciences of Ukraine, Ukraine; Science and Technology Facilities Council (STFC), United Kingdom; National Science Foundation of the United States of America (NSF) and United States Department of Energy, Office of Nuclear Physics (DOE NP), United States of America. In addition, individual groups or members have received support from: Czech Science Foundation (grant no. 23-07499S), Czech Republic; European Research Council, Strong 2020 - Horizon 2020 (grant nos. 950692, 824093), European Union; ICSC - Centro Nazionale di Ricerca in High Performance Computing, Big Data and Quantum Computing, European Union - NextGenerationEU; Academy of Finland (Center of Excellence in Quark Matter) (grant nos. 346327, 346328), Finland.

References

- [1] E. Shuryak, “Strongly coupled quark-gluon plasma in heavy ion collisions”, *Rev. Mod. Phys.* **89** (2017) 035001, arXiv:1412.8393 [hep-ph].
- [2] P. Braun-Munzinger, V. Koch, T. Schäfer, and J. Stachel, “Properties of hot and dense matter from relativistic heavy ion collisions”, *Phys. Rept.* **621** (2016) 76–126, arXiv:1510.00442 [nucl-th].
- [3] W. Busza, K. Rajagopal, and W. van der Schee, “Heavy Ion Collisions: The Big Picture, and the Big Questions”, *Ann. Rev. Nucl. Part. Sci.* **68** (2018) 339–376, arXiv:1802.04801 [hep-ph].
- [4] Y. Mehtar-Tani and G. Wolschin, “Baryon stopping and saturation physics in relativistic collisions”, *Phys. Rev. C* **80** (2009) 054905, arXiv:0907.5444 [hep-ph].
- [5] L. D. McLerran and R. Venugopalan, “Computing quark and gluon distribution functions for very large nuclei”, *Phys. Rev. D* **49** (1994) 2233–2241, arXiv:hep-ph/9309289.
- [6] S. E. Vance, M. Gyulassy, and X. N. Wang, “Baryon junction stopping at the SPS and RHIC via HIJING/B”, *Nucl. Phys. A* **638** (1998) 395C–398C, arXiv:nucl-th/9802036.
- [7] A. Capella and B. Z. Kopeliovich, “Novel mechanism of nucleon stopping in heavy ion collisions”, *Phys. Lett. B* **381** (1996) 325–330, arXiv:hep-ph/9603279.
- [8] F. Videbaek, “Stopping and baryon transport in heavy ion reactions”, *J. Phys. Conf. Ser.* **50** (2006) 134–141, arXiv:nucl-ex/0505010.
- [9] V. Topor Pop, J. Barrette, C. Gale, S. Jeon, and M. Gyulassy, “Stopping Power from SPS to LHC energies”, arXiv:0705.2759 [hep-ph].
- [10] J. Hoelck and G. Wolschin, “Baryon stopping as a relativistic Markov process in phase space”, *Phys. Rev. Res.* **2** (2020) 033409, arXiv:2009.08913 [nucl-th].
- [11] H. Elfner and B. Müller, “The exploration of hot and dense nuclear matter: introduction to relativistic heavy-ion physics”, *J. Phys. G* **50** (2023) 103001, arXiv:2210.12056 [nucl-th].

- [12] M. J. Fromerth, I. Kuznetsova, L. Labun, J. Letessier, and J. Rafelski, “From Quark-Gluon Universe to Neutrino Decoupling: $200 < T < 2\text{MeV}$ ”, *Acta Phys. Polon. B* **43** (2012) 2261–2284, arXiv:1211.4297 [nucl-th].
- [13] P. Braun-Munzinger and J. Stachel, “Dynamics of ultrarelativistic nuclear collisions with heavy beams: An Experimental overview”, *Nucl. Phys. A* **638** (1998) 3–18, arXiv:nucl-ex/9803015.
- [14] J. Cleymans and K. Redlich, “Unified description of freezeout parameters in relativistic heavy ion collisions”, *Phys. Rev. Lett.* **81** (1998) 5284–5286, arXiv:nucl-th/9808030.
- [15] P. Braun-Munzinger, K. Redlich, and J. Stachel, “Particle production in heavy ion collisions”, in *Quark–Gluon Plasma 3*, pp. 491–599. World Scientific, 2004. arXiv:nucl-th/0304013.
- [16] J. Cleymans, H. Oeschler, K. Redlich, and S. Wheaton, “Comparison of chemical freeze-out criteria in heavy-ion collisions”, *Phys. Rev. C* **73** (2006) 034905, arXiv:hep-ph/0511094.
- [17] P. Braun-Munzinger and J. Wambach, “The Phase Diagram of Strongly-Interacting Matter”, *Rev. Mod. Phys.* **81** (2009) 1031–1050, arXiv:0801.4256 [hep-ph].
- [18] V. Vovchenko and H. Stoecker, “Examination of the sensitivity of the thermal fits to heavy-ion hadron yield data to the modeling of the eigenvolume interactions”, *Phys. Rev. C* **95** (2017) 044904, arXiv:1606.06218 [hep-ph].
- [19] R. Hagedorn and K. Redlich, “Statistical Thermodynamics in Relativistic Particle and Ion Physics: Canonical or Grand Canonical?”, *Z. Phys. C* **27** (1985) 541.
- [20] K. Redlich, J. Cleymans, H. Oeschler, and A. Tounsi, “Conservation laws and particle production in heavy ion collisions”, *AIP Conf. Proc.* **594** (2002) 318–329, arXiv:hep-ph/0110337.
- [21] A. Bazavov *et al.*, “Freeze-out Conditions in Heavy Ion Collisions from QCD Thermodynamics”, *Phys. Rev. Lett.* **109** (2012) 192302, arXiv:1208.1220 [hep-lat].
- [22] V. Vovchenko and H. Stoecker, “Thermal-FIST: A package for heavy-ion collisions and hadronic equation of state”, *Comput. Phys. Commun.* **244** (2019) 295–310, arXiv:1901.05249 [nucl-th].
- [23] J. Stachel and P. Braun-Munzinger, “Stopping in High-energy Nucleus Nucleus Collisions: Analysis in the Landau Hydrodynamic Model”, *Phys. Lett. B* **216** (1989) 1–6.
- [24] P. Braun-Munzinger, J. Stachel, J. P. Wessels, and N. Xu, “Thermal equilibration and expansion in nucleus-nucleus collisions at the AGS”, *Phys. Lett. B* **344** (1995) 43–48, arXiv:nucl-th/9410026.
- [25] **E802** Collaboration, L. Ahle *et al.*, “Anti-proton production in Au + Au collisions at 11.7 AGeV/c”, *Phys. Rev. Lett.* **81** (1998) 2650–2654, arXiv:nucl-ex/9709005.
- [26] **NA49** Collaboration, F. Siklér *et al.*, “Hadron production in nuclear collisions from the NA49 experiment at 158 GeV/c/A”, *Nucl. Phys. A* **661** (1999) 45–54.
- [27] P. Braun-Munzinger, I. Heppe, and J. Stachel, “Chemical equilibration in Pb + Pb collisions at the SPS”, *Phys. Lett. B* **465** (1999) 15–20, arXiv:nucl-th/9903010.
- [28] F. Becattini, J. Cleymans, A. Keranen, E. Suhonen, and K. Redlich, “Features of particle multiplicities and strangeness production in central heavy ion collisions between 1.7 AGeV/c and 158 AGeV/c”, *Phys. Rev. C* **64** (2001) 024901, arXiv:hep-ph/0002267.

- [29] P. Braun-Munzinger and J. Stachel, “Particle ratios, equilibration, and the QCD phase boundary”, *J. Phys. G* **28** (2002) 1971–1976, arXiv:nucl-th/0112051.
- [30] **STAR** Collaboration, C. Adler *et al.*, “Midrapidity anti-proton to proton ratio from Au + Au collisions at $\sqrt{s_{NN}} = 130$ GeV”, *Phys. Rev. Lett.* **86** (2001) 4778, arXiv:nucl-ex/0104022. [Erratum: Phys.Rev.Lett. 90, 119903 (2003)].
- [31] **BRAHMS** Collaboration, I. G. Bearden *et al.*, “Rapidity dependence of anti-proton to proton ratios in Au+Au collisions at $\sqrt{s_{NN}} = 130$ GeV”, *Phys. Rev. Lett.* **87** (2001) 112305, arXiv:nucl-ex/0106011.
- [32] P. Braun-Munzinger, D. Magestro, K. Redlich, and J. Stachel, “Hadron production in Au-Au collisions at RHIC”, *Phys. Lett. B* **518** (2001) 41–46, arXiv:hep-ph/0105229.
- [33] D. Magestro, “Evidence for chemical equilibration at RHIC”, *J. Phys. G* **28** (2002) 1745–1752, arXiv:hep-ph/0112178.
- [34] F. Becattini, M. Gazdzicki, A. Keranen, J. Manninen, and R. Stock, “Chemical equilibrium study in nucleus nucleus collisions at relativistic energies”, *Phys. Rev. C* **69** (2004) 024905, arXiv:hep-ph/0310049.
- [35] **ALICE** Collaboration, B. Abelev *et al.*, “Centrality dependence of π , K, p production in Pb-Pb collisions at $\sqrt{s_{NN}} = 2.76$ TeV”, *Phys. Rev. C* **88** (2013) 044910, arXiv:1303.0737 [hep-ex].
- [36] A. Andronic, P. Braun-Munzinger, K. Redlich, and J. Stachel, “Decoding the phase structure of QCD via particle production at high energy”, *Nature* **561** (2018) 321–330, arXiv:1710.09425 [nucl-th].
- [37] A. Andronic, P. Braun-Munzinger, B. Friman, P. M. Lo, K. Redlich, and J. Stachel, “The thermal proton yield anomaly in Pb-Pb collisions at the LHC and its resolution”, *Phys. Lett. B* **792** (2019) 304–309, arXiv:1808.03102 [hep-ph].
- [38] A. Andronic, P. Braun-Munzinger, K. Redlich, and J. Stachel, “Hadron yields in central nucleus-nucleus collisions, the statistical hadronization model and the QCD phase diagram”, in *Criticality in QCD and the Hadron Resonance Gas*. 1, 2021. arXiv:2101.05747 [nucl-th].
- [39] **NA49** Collaboration, H. Appelshäuser *et al.*, “Xi and anti-xi production in 158-GeV / nucleon Pb + Pb collisions”, *Phys. Lett. B* **444** (1998) 523–530, arXiv:nucl-ex/9810005.
- [40] **E802** Collaboration, L. Ahle *et al.*, “Kaon production in au+au collisions at 11.6A GeV/c”, *Phys. Rev. C* **58** (Dec, 1998) 3523–3538.
- [41] **E802** Collaboration, L. Ahle *et al.*, “Proton and deuteron production in Au + Au reactions at 11.6/A-GeV/c”, *Phys. Rev. C* **60** (1999) 064901.
- [42] **E866, E917** Collaboration, L. Ahle *et al.*, “Excitation function of K+ and pi+ production in Au + Au reactions at 2 AGeV to 10 AGeV”, *Phys. Lett. B* **476** (2000) 1–8, arXiv:nucl-ex/9910008.
- [43] **E877** Collaboration, J. Barrette *et al.*, “Proton and pion production in Au + Au collisions at 10.8A-GeV/c”, *Phys. Rev. C* **62** (2000) 024901, arXiv:nucl-ex/9910004.
- [44] S. Afanasiev *et al.*, “Production of ϕ mesons in p+p, p+Pb and central Pb+Pb collisions at $E_{\text{beam}}=158$ AGeV”, *Physics Letters B* **491** (2000) 59–66.
- [45] **E866, E917** Collaboration, L. Ahle *et al.*, “An Excitation function of K- and K+ production in Au + Au reactions at the AGS”, *Phys. Lett. B* **490** (2000) 53–60, arXiv:nucl-ex/0008010.

- [46] **E917** Collaboration, B. B. Back *et al.*, “Baryon rapidity loss in relativistic Au+Au collisions”, *Phys. Rev. Lett.* **86** (2001) 1970–1973, arXiv:nucl-ex/0003007.
- [47] **E895** Collaboration, C. Pinkenburg *et al.*, “Production and collective behavior of strange particles in Au + Au collisions at 2–8 AGeV”, *Nucl. Phys. A* **698** (2002) 495–498, arXiv:nucl-ex/0104025.
- [48] **E895** Collaboration, J. L. Klay *et al.*, “Longitudinal flow from 2 AGeV to 8 AGeV Au+Au collisions at the Brookhaven AGS”, *Phys. Rev. Lett.* **88** (2002) 102301, arXiv:nucl-ex/0111006.
- [49] S. Albergo *et al.*, “ Λ Spectra in 11.6 AGeV/c Au-Au Collisions”, *Phys. Rev. Lett.* **88** (Jan, 2002) 062301.
- [50] **STAR** Collaboration, C. Adler *et al.*, “Kaon production and kaon to pion ratio in Au+Au collisions at $\sqrt{s_{NN}} = 130$ GeV”, *Phys. Lett. B* **595** (2004) 143–150, arXiv:nucl-ex/0206008.
- [51] **STAR** Collaboration, C. Adler *et al.*, “ $K^*(892)^0$ production in relativistic heavy ion collisions at $\sqrt{s_{NN}} = 130$ GeV”, *Phys. Rev. C* **66** (2002) 061901, arXiv:nucl-ex/0205015.
- [52] **NA49** Collaboration, S. V. Afanasiev *et al.*, “Energy dependence of pion and kaon production in central Pb + Pb collisions”, *Phys. Rev. C* **66** (2002) 054902, arXiv:nucl-ex/0205002.
- [53] **PHENIX** Collaboration, K. Adcox *et al.*, “Measurement of the Lambda and anti-Lambda particles in Au+Au collisions at $\sqrt{s_{NN}} = 130$ GeV”, *Phys. Rev. Lett.* **89** (2002) 092302, arXiv:nucl-ex/0204007.
- [54] **STAR** Collaboration, C. Adler *et al.*, “Midrapidity phi production in Au + Au collisions at $\sqrt{s_{NN}} = 130$ GeV”, *Phys. Rev. C* **65** (2002) 041901.
- [55] **NA44** Collaboration, I. G. Bearden *et al.*, “Particle production in central Pb + Pb collisions at 158-A-GeV/c”, *Phys. Rev. C* **66** (2002) 044907, arXiv:nucl-ex/0202019.
- [56] **E917** Collaboration, B. B. Back *et al.*, “Production of phi mesons in Au+Au collisions at 11.7-A-GeV/c”, *Phys. Rev. C* **69** (2004) 054901, arXiv:nucl-ex/0304017.
- [57] **E895** Collaboration, J. L. Klay *et al.*, “Charged pion production in 2 to 8 agev central au+au collisions”, *Phys. Rev. C* **68** (2003) 054905, arXiv:nucl-ex/0306033.
- [58] **E895** Collaboration, P. Chung *et al.*, “Near threshold production of the multistrange Ξ^- hyperon”, *Phys. Rev. Lett.* **91** (2003) 202301, arXiv:nucl-ex/0302021.
- [59] **PHENIX** Collaboration, K. Adcox *et al.*, “Single identified hadron spectra from $\sqrt{s_{NN}} = 130$ GeV Au+Au collisions”, *Phys. Rev. C* **69** (2004) 024904, arXiv:nucl-ex/0307010.
- [60] **NA49 Collaboration** Collaboration, T. Anticic *et al.*, “Energy and centrality dependence of deuteron and proton production in Pb + Pb collisions at relativistic energies”, *Phys. Rev. C* **69** (Feb, 2004) 024902.
- [61] **NA49** Collaboration, T. Anticic *et al.*, “Lambda and anti-Lambda production in central Pb - Pb collisions at 40-A-GeV, 80-A-GeV and 158-A-GeV”, *Phys. Rev. Lett.* **93** (2004) 022302, arXiv:nucl-ex/0311024.
- [62] **PHENIX** Collaboration, S. S. Adler *et al.*, “Identified charged particle spectra and yields in Au+Au collisions at $\sqrt{s_{NN}} = 200$ GeV”, *Phys. Rev. C* **69** (2004) 034909, arXiv:nucl-ex/0307022.

- [63] **STAR** Collaboration, J. Adams *et al.*, “Multistrange baryon production in Au-Au collisions at $\sqrt{s_{NN}} = 130$ GeV”, *Phys. Rev. Lett.* **92** (2004) 182301, arXiv:nucl-ex/0307024.
- [64] **STAR** Collaboration, J. Adams *et al.*, “Identified particle distributions in pp and Au+Au collisions at $\sqrt{s_{NN}} = 200$ GeV”, *Phys. Rev. Lett.* **92** (2004) 112301, arXiv:nucl-ex/0310004.
- [65] **NA49** Collaboration, C. Alt *et al.*, “Omega- and anti-Omega+ production in central Pb + Pb collisions at 40-AGeV and 158-AGeV”, *Phys. Rev. Lett.* **94** (2005) 192301, arXiv:nucl-ex/0409004.
- [66] **NA57** Collaboration, F. Antinori *et al.*, “Energy dependence of hyperon production in nucleus nucleus collisions at SPS”, *Phys. Lett. B* **595** (2004) 68–74, arXiv:nucl-ex/0403022.
- [67] **STAR** Collaboration, J. Adams *et al.*, “K(892)* resonance production in Au+Au and p+p collisions at $\sqrt{s_{NN}} = 200$ GeV at STAR”, *Phys. Rev. C* **71** (2005) 064902, arXiv:nucl-ex/0412019.
- [68] **PHENIX** Collaboration, S. S. Adler *et al.*, “Production of ϕ mesons at mid-rapidity in $\sqrt{s_{NN}} = 200$ GeV Au+Au collisions at RHIC”, *Phys. Rev. C* **72** (2005) 014903, arXiv:nucl-ex/0410012.
- [69] **PHENIX** Collaboration, S. S. Adler *et al.*, “Deuteron and antideuteron production in Au + Au collisions at $\sqrt{s_{NN}} = 200$ GeV”, *Phys. Rev. Lett.* **94** (2005) 122302, arXiv:nucl-ex/0406004.
- [70] **STAR** Collaboration, J. Adams *et al.*, “phi meson production in Au + Au and p+p collisions at $\sqrt{s_{NN}} = 200$ GeV”, *Phys. Lett. B* **612** (2005) 181–189, arXiv:nucl-ex/0406003.
- [71] A. E. M. Billmeier and (for the STAR Collaboration), “Strange and multi-strange particle ratios in p + p reactions at gev at rhic”, *Journal of Physics G: Nuclear and Particle Physics* **30** (Dec, 2003) S363.
- [72] **STAR** Collaboration, H.-b. Zhang, “ Δ , K^* and rho resonance production and their probing of freezeout dynamics at RHIC”, in *17th International Conference on Ultra Relativistic Nucleus-Nucleus Collisions (Quark Matter 2004)*. 3, 2004. arXiv:nucl-ex/0403010.
- [73] **STAR** Collaboration, O. Y. Barannikova, “Probing collision dynamics at RHIC”, in *17th International Conference on Ultra Relativistic Nucleus-Nucleus Collisions (Quark Matter 2004)*. 3, 2004. arXiv:nucl-ex/0403014.
- [74] **NA57** Collaboration, F. Antinori *et al.*, “Rapidity distributions around mid-rapidity of strange particles in Pb-Pb collisions at 158-A-GeV/c”, *J. Phys. G* **31** (2005) 1345–1357, arXiv:nucl-ex/0509009.
- [75] **BRAHMS** Collaboration, I. Arsene *et al.*, “Centrality dependent particle production at $y=0$ and $y \sim 1$ in Au + Au collisions at $\sqrt{s_{NN}} = 200$ GeV”, *Phys. Rev. C* **72** (2005) 014908, arXiv:nucl-ex/0503010.
- [76] A. Andronic, P. Braun-Munzinger, and J. Stachel, “Hadron production in central nucleus-nucleus collisions at chemical freeze-out”, *Nucl. Phys. A* **772** (2006) 167–199, arXiv:nucl-th/0511071.
- [77] A. Andronic, P. Braun-Munzinger, and J. Stachel, “Thermal hadron production in relativistic nuclear collisions: The Hadron mass spectrum, the horn, and the QCD phase transition”, *Phys. Lett. B* **673** (2009) 142–145, arXiv:0812.1186 [nucl-th]. [Erratum: Phys.Lett.B 678, 516 (2009)].

- [78] P. Alba, W. Alberico, R. Bellwied, M. Bluhm, V. Mantovani Sarti, M. Nahrgang, and C. Ratti, “Freeze-out conditions from net-proton and net-charge fluctuations at RHIC”, *Phys. Lett. B* **738** (2014) 305–310, arXiv:1403.4903 [hep-ph].
- [79] STAR Collaboration, L. Adamczyk *et al.*, “Bulk Properties of the Medium Produced in Relativistic Heavy-Ion Collisions from the Beam Energy Scan Program”, *Phys. Rev. C* **96** (2017) 044904, arXiv:1701.07065 [nucl-ex].
- [80] ALICE Collaboration, K. Aamodt *et al.*, “Midrapidity antiproton-to-proton ratio in pp collisions at $\sqrt{s} = 0.9$ and 7 TeV measured by the ALICE experiment”, *Phys. Rev. Lett.* **105** (2010) 072002, arXiv:1006.5432 [hep-ex].
- [81] J. Cleymans, I. Kraus, H. Oeschler, K. Redlich, and S. Wheaton, “Statistical model predictions for particle ratios at $\sqrt{s_{\text{NN}}} = 5.5$ TeV”, *Phys. Rev. C* **74** (2006) 034903, arXiv:hep-ph/0604237.
- [82] ALICE Collaboration, S. Acharya *et al.*, “Production of charged pions, kaons, and (anti-)protons in Pb-Pb and inelastic *pp* collisions at $\sqrt{s_{\text{NN}}} = 5.02$ TeV”, *Phys. Rev. C* **101** (2020) 044907, arXiv:1910.07678 [nucl-ex].
- [83] ALICE Collaboration, E. Abbas *et al.*, “Mid-rapidity anti-baryon to baryon ratios in pp collisions at $\sqrt{s} = 0.9, 2.76$ and 7 TeV measured by ALICE”, *Eur. Phys. J. C* **73** (2013) 2496, arXiv:1305.1562 [nucl-ex].
- [84] ALICE Collaboration, S. Acharya *et al.*, “Measurement of the low-energy antideuteron inelastic cross section”, *Phys. Rev. Lett.* **125** (2020) 162001, arXiv:2005.11122 [nucl-ex].
- [85] ALICE Collaboration, K. Aamodt *et al.*, “The ALICE experiment at the CERN LHC”, *JINST* **3** (2008) S08002.
- [86] ALICE Collaboration, B. B. Abelev *et al.*, “Performance of the ALICE Experiment at the CERN LHC”, *Int. J. Mod. Phys. A* **29** (2014) 1430044, arXiv:1402.4476 [nucl-ex].
- [87] ALICE Collaboration, E. Abbas *et al.*, “Performance of the ALICE VZERO system”, *JINST* **8** (2013) P10016, arXiv:1306.3130 [nucl-ex].
- [88] ALICE Collaboration, “Centrality determination in heavy ion collisions”, *ALICE-PUBLIC-2018-011* (2018) . <https://cds.cern.ch/record/2636623>.
- [89] ALICE Collaboration, K. Aamodt *et al.*, “Alignment of the ALICE Inner Tracking System with cosmic-ray tracks”, *JINST* **5** (2010) P03003, arXiv:1001.0502 [physics.ins-det].
- [90] J. Alme *et al.*, “The ALICE TPC, a large 3-dimensional tracking device with fast readout for ultra-high multiplicity events”, *Nucl. Instrum. Meth. A* **622** (2010) 316–367, arXiv:1001.1950 [physics.ins-det].
- [91] ALICE Collaboration, J. Adam *et al.*, “Production of light nuclei and anti-nuclei in pp and Pb-Pb collisions at energies available at the CERN Large Hadron Collider”, *Phys. Rev. C* **93** (2016) 024917, arXiv:1506.08951 [nucl-ex].
- [92] ALICE Collaboration, S. Acharya *et al.*, “Light (anti)nuclei production in Pb-Pb collisions at $\sqrt{s_{\text{NN}}} = 5.02$ TeV”, *Phys. Rev. C* **107** (2023) 064904, arXiv:2211.14015 [nucl-ex].
- [93] X.-N. Wang and M. Gyulassy, “HIJING: A Monte Carlo model for multiple jet production in p p, p A and A A collisions”, *Phys. Rev. D* **44** (1991) 3501–3516.

- [94] GEANT4 Collaboration, S. Agostinelli *et al.*, “GEANT4—a simulation toolkit”, *Nucl. Instrum. Meth. A* **506** (2003) 250–303.
- [95] F. F. Chen, C. P. Leavitt, and A. M. Shapiro, “Attenuation Cross Sections for 860-Mev Protons”, *Physical Review* **99** (1955) 857.
- [96] N. E. Booth, B. Ledley, D. Walker, and D. H. White, “Nuclear cross sections for 900 MeV protons.”, *Proc. Physical Society (London), Section A* **70** (1957) 209.
- [97] N. T. Porile, “Simple Nuclear Reactions of Indium with 30 and 2.9 GeV Protons”, *Physical Review* **128** (1962) 1916.
- [98] O. Artun, *et al.*, “Multinucleon Removal Induced by High-Energy Protons”, *Phys. Rev. Lett.* **35** (1975) 773.
- [99] M. E. Sadler, P. P. Singh, J. Jastrzebski, L. L. Rutledge, J. , and R. E. Segel, “Interaction of 80-164 MeV Protons with Nickel Isotopes”, *Phys. Rev. C* **21** (1980) 2303.
- [100] D. Ashery, I. Navon, G. Azuelos, H. K. Walter, H. J. Pfeiffer, and F. W. Schlegel, “True Absorption and Scattering of Pions on Nuclei”, *Phys. Rev. C* **23** (1981) 2173–2185.
- [101] K. Nakamura, J. Chiba, T. Fujii, H. Iwasaki, T. Kageyama, S. Kuribayashi, T. Sumiyoshi, T. Takeda, H. Ikeda, and Y. Takada, “Absorption and Forward Scattering of Antiprotons by C, Al, and Cu Nuclei in the Region 470-880 MeV/c”, *Phys. Rev. Lett.* **52** (1984) 731–734.
- [102] J. A. McGill, G. W. Hoffmann, M. L. Barlett, R. W. Ferguson, E. C. Milner, R. E. Chrien, R. J. Sutter, T. Kozlowski, and R. L. Stearns, “Proton + Nucleus Inclusive (p,p’) Scattering at 800 MeV”, *Phys. Rev. C* **29** (1984) 204.
- [103] N. G. Zaitseva, E. Rurarz, M. Vobecky, K. H. Hwan, K. Nowak, T. Tethal, V. A. Khalkin, and L. M. Popinenkova, “Excitation Function and Yield for ^{97}Ru Production in $^{99}\text{Tc}(p,3n)^{97}\text{Ru}$ Reaction in 20-100 MeV Proton Energy Range”, *Radiochimica Acta* **56** (1992) 59.
- [104] V. F. Kuzichev, Y. B. Lepikhin, and V. A. Smirnitsky, “The Anti-proton - nuclei annihilation cross-section at the momentum range from 0.70 GeV/c to 2.5 GeV/c”, *Nucl. Phys. A* **576** (1994) 581–602.
- [105] C. M. Herbach, *et al.*, “Systematic investigation of 1.2 GeV proton-induced spallation reactions on targets between Al and U”, *Nucl. Instrum. Methods in Physics Res., Sect. A* **562** (2006) 729.
- [106] M. Zamani, S. Stoulos, M. Fragopoulou, M. Manolopoulou, and M. Krivopustov, “Indirect measurement of inelastic cross section of relativistic protons in Pb target”, *Annals of Nuclear Energy* **37** (2010) 923.
- [107] D. W. Bardayan, *et al.*, “Inelastic $^{17}\text{F}(p,p)^{17}\text{F}$ scattering at $E_{c.m.}=3$ MeV and the $^{14}\text{O}(\alpha,p)^{17}\text{F}$ reaction rate”, *Phys. Rev. C* **81** (2010) 065802.
- [108] ALICE Collaboration, S. Acharya *et al.*, “Measurement of anti- ^3He nuclei absorption in matter and impact on their propagation in the Galaxy”, *Nature Phys.* **19** (2023) 61–71, arXiv:2202.01549 [nucl-ex].
- [109] ALICE Collaboration, S. Acharya *et al.*, “Measurement of the low-energy antitriton inelastic cross section”, *Phys. Lett. B* **848** (2024) 138337, arXiv:2307.03603 [nucl-ex].
- [110] ALICE Collaboration, J. Adam *et al.*, “ $^3_{\Lambda}\text{H}$ and $^3_{\Lambda}\bar{\text{H}}$ production in Pb-Pb collisions at $\sqrt{s_{NN}} = 2.76$ TeV”, *Phys. Lett. B* **754** (2016) 360–372, arXiv:1506.08453 [nucl-ex].

- [111] ALICE Collaboration, S. Acharya *et al.*, “ ${}^3_{\Lambda}\text{H}$ and ${}^3_{\Lambda}\bar{\text{H}}$ lifetime measurement in Pb–Pb collisions at $\sqrt{s_{\text{NN}}} = 5.02$ TeV via two-body decay”, *Phys. Lett. B* **797** (2019) 134905, arXiv:1907.06906 [nucl-ex].
- [112] ALICE Collaboration, S. Acharya *et al.*, “Hypertriton Production in p–Pb Collisions at $\sqrt{s_{\text{NN}}}=5.02$ TeV”, *Phys. Rev. Lett.* **128** (2022) 252003, arXiv:2107.10627 [nucl-ex].
- [113] ALICE Collaboration, S. Acharya *et al.*, “Measurement of the Lifetime and Λ Separation Energy of ${}^3_{\Lambda}\text{H}$ ”, *Phys. Rev. Lett.* **131** (2023) 102302, arXiv:2209.07360 [nucl-ex].
- [114] ALICE Collaboration, B. Abelev *et al.*, “Multi-strange baryon production in pp collisions at $\sqrt{s} = 7$ TeV with ALICE”, *Phys. Lett. B* **712** (2012) 309–318, arXiv:1204.0282 [nucl-ex].
- [115] ALICE Collaboration, B. B. Abelev *et al.*, “Multi-strange baryon production at mid-rapidity in Pb–Pb collisions at $\sqrt{s_{\text{NN}}} = 2.76$ TeV”, *Phys. Lett. B* **728** (2014) 216–227, arXiv:1307.5543 [nucl-ex]. [Erratum: *Phys.Lett.B* 734, 409–410 (2014)].
- [116] ALICE Collaboration, J. Adam *et al.*, “Multi-strange baryon production in p–Pb collisions at $\sqrt{s_{\text{NN}}} = 5.02$ TeV”, *Phys. Lett. B* **758** (2016) 389–401, arXiv:1512.07227 [nucl-ex].
- [117] T. Chen and C. Guestrin, “Xgboost: A scalable tree boosting system”, in *Proceedings of the 22nd ACM SIGKDD International Conference on Knowledge Discovery and Data Mining, KDD ’16*, p. 785–794. Association for Computing Machinery, New York, NY, USA, 2016.
- [118] K. S. Cranmer, “Kernel estimation in high-energy physics”, *Comput. Phys. Commun.* **136** (2001) 198–207, arXiv:hep-ex/0011057.
- [119] W. Verkerke and D. P. Kirkby, “The RooFit toolkit for data modeling”, *eConf C0303241* (2003) MOLT007, arXiv:physics/0306116.
- [120] ALICE Collaboration, J. Adam *et al.*, “Quarkonium signal extraction in ALICE”, *ALICE-PUBLIC-2015-006* (2015). <https://cds.cern.ch/record/2060096/>.
- [121] V. Vovchenko, M. I. Gorenstein, and H. Stoecker, “Finite resonance widths influence the thermal-model description of hadron yields”, *Phys. Rev. C* **98** (2018) 034906, arXiv:1807.02079 [nucl-th].
- [122] ALICE Collaboration, S. Acharya *et al.*, “The ALICE experiment: a journey through QCD”, *Eur. Phys. J. C* **84** (2024) 813, arXiv:2211.04384 [nucl-ex].
- [123] S. Borsanyi, Z. Fodor, J. N. Guenther, R. Kara, S. D. Katz, P. Parotto, A. Pasztor, C. Ratti, and K. K. Szabo, “QCD Crossover at Finite Chemical Potential from Lattice Simulations”, *Phys. Rev. Lett.* **125** (2020) 052001, arXiv:2002.02821 [hep-lat].
- [124] STAR Collaboration, B. I. Abelev *et al.*, “Systematic Measurements of Identified Particle Spectra in pp, d+Au and Au+Au Collisions from STAR”, *Phys. Rev. C* **79** (2009) 034909, arXiv:0808.2041 [nucl-ex].
- [125] V. Vovchenko, B. Dönigus, and H. Stoecker, “Canonical statistical model analysis of p–p, p–Pb, and Pb–Pb collisions at energies available at the CERN Large Hadron Collider”, *Phys. Rev. C* **100** (2019) 054906, arXiv:1906.03145 [hep-ph].
- [126] J. Cleymans, P. M. Lo, K. Redlich, and N. Sharma, “Multiplicity dependence of (multi)strange baryons in the canonical ensemble with phase shift corrections”, *Phys. Rev. C* **103** (2021) 014904, arXiv:2009.04844 [hep-ph].

- [127] J. Cleymans, H. Oeschler, and K. Redlich, “Statistical model description of K⁺ and K⁻ production between 1 AGeV to 10 AGeV”, *Phys. Lett. B* **485** (2000) 27–31, arXiv:nucl-th/0004025.
- [128] J. D. Brandenburg, N. Lewis, P. Tribedy, and Z. Xu, “Search for baryon junctions in photonuclear processes and isobar collisions at RHIC”, *Eur. Phys. J. C* **84** (2024) 590, arXiv:2205.05685 [hep-ph].
- [129] E. Schnedermann, J. Sollfrank, and U. W. Heinz, “Thermal phenomenology of hadrons from 200 AGeV S+S collisions”, *Phys. Rev. C* **48** (1993) 2462–2475, arXiv:nucl-th/9307020.

A Antiparticle-to-particle ratios

A.1 Particle identification of tracked species

The particle identification (PID) of charged pions, protons, ${}^3\text{He}$, and tritons is performed by measuring the specific energy loss (dE/dx) in both the TPC and the ITS, and particle velocity depending on the transverse momentum of the measured particles with the Time-Of-Flight detector (TOF). Due to its electric charge $Z = 2$, ${}^3\text{He}$ is identified using the TPC dE/dx within $|n\sigma^{\text{TPC}}| < 3$, where $n\sigma$ is the deviation of the measured dE/dx from the expected one, normalized to the experimental resolution. A similar approach is applied to protons for $p_T < 1$ GeV/ c after a preliminary $|n\sigma^{\text{ITS}}| < 3$ selection, which is required to reduce the electron contamination. Higher- p_T protons, pions, and tritons are identified using TOF after preliminary TPC PID selections. These PID pre-selections lead to a signal loss smaller than 0.5% taken into account by the efficiency corrections computed via Monte Carlo simulations. The main contamination to the charged pion and proton PID is due to charged kaons and electrons. In the light-nuclei sector, the triton PID is mainly contaminated by deuterons, while tritons slightly affect the ${}^3\text{He}$ PID for $p_T < 3$ GeV/ c . The contribution of such misidentified tracks is estimated by fitting the corresponding $n\sigma^{\text{TPC}}$ and $n\sigma^{\text{TOF}}$ distributions. The $n\sigma^{\text{TPC}}$ or $n\sigma^{\text{TOF}}$ background distributions are fitted outside of the signal window. Their extrapolation within the signal region is integrated to statistically subtract the contamination due to either misidentified particles or the mismatch of TPC tracks and TOF space points.

A.2 Machine Learning analysis of Ω and ${}^3_{\Lambda}\text{H}$

The Machine Learning (ML) selection of Ω and ${}^3_{\Lambda}\text{H}$ candidates is based on Boosted Decision Trees (BDT). The optimization of the BDT internal parameters is performed using samples of correctly classified signal and background candidates. The signal sample is built from simulated candidates injected on top of a HIJING Pb–Pb event with a Blast-wave p_T distribution [129] derived from the measured production of light flavor hadrons for Ω [82] and of ${}^3\text{He}$ for ${}^3_{\Lambda}\text{H}$ [92]. The background ${}^3_{\Lambda}\text{H}$ candidates are obtained in the data from same-sign combinations of ${}^3\text{He}$ and π tracks. For Ω^- , all the candidates with an invariant-mass deviating more than 7σ from the nominal Ω^- mass are considered as background candidates, with $\sigma \approx 1.7$ MeV/ c^2 being the invariant-mass resolution in the data. The same training variables used in previous analyses are employed for ${}^3_{\Lambda}\text{H}$ [112, 113]: the cosine of the pointing angle $\cos(\theta_p)$ (i.e., the angle between the reconstructed candidate momentum and the straight line connecting the production and decay vertices), the DCA between the decay tracks and the primary vertex (PV), and between the two tracks themselves, the number of TPC space points for the ${}^3\text{He}$ track, and the $n\sigma^{\text{TPC}}$ of the decay tracks. For the Ω^- , the BDT input variables include the DCA of the K^- , π^- and p to the PV, the DCA of the reconstructed Λ to the PV, the minimum distance between the π^- and p, and between the K^- and Λ . The $\cos(\theta_p)$ for both the Ω^- and Λ , and the $n\sigma^{\text{TPC}}$ for p, are also used as BDT input variables. Signal candidates are selected requiring a BDT output score larger than a preset threshold. For ${}^3_{\Lambda}\text{H}$, the threshold is optimized by maximizing the expected signal significance; for the Ω^- , a BDT signal selection efficiency of 50% is required, as it ensures a consistent BDT response in data and MC.

A.3 Efficiency and absorption corrections

The efficiency corrections applied in this Letter take into account the tracking and candidate-selection efficiencies, including PID. Charged pions, protons, and tritons are selected with an efficiency of about 40% when requiring TOF PID, while protons having $p_T < 1$ GeV/ c and ${}^3\text{He}$ candidates are selected with an efficiency of approximately 70%. For antiproton, antitriton, and ${}^3\overline{\text{He}}$ candidates, the obtained efficiencies are lower than those of their respective charge-conjugates by about 5% to 10% due to their larger absorption cross sections inside the ALICE apparatus. For Ω^- baryons, the efficiency of the preliminary selections is about 5%, while the BDT signal-selection efficiency is about 50%. For ${}^3_{\Lambda}\text{H}$, these two efficiencies are about 30% and 70%, respectively.

The modeling of the absorption cross sections in GEANT 4 is improved by using the available measurements of absorption cross sections in different materials [95–109]. Dedicated correction factors are computed as the ratios between the efficiencies computed using either the default parameterizations or those re-tuned on the experimental data. For charged pions and protons, the measurements obtained in lower energy experiments are used, while for tritons and ${}^3\text{He}$ the available ALICE measurements are employed. For the light (anti)nuclei, the observed effect is between 1% and 3% across the analysed p_{T} range. The uncertainties on the measured cross sections are propagated to the antiparticle-to-particle ratios as centrality-correlated sources of systematic uncertainties. The resulting uncertainties are reported in Table A.1. For the ${}^3_{\Lambda}\text{H}$, an absorption factor is computed to correct for undetected hypernuclei that are absorbed in the apparatus before decaying. A sample of simulated ${}^3\text{He}$ candidates is used to approximate the absorption of ${}^3_{\Lambda}\text{H}$ inside the ALICE apparatus. The absorbed fraction is about 6% and 4% for ${}^3_{\Lambda}\bar{\text{H}}$ and ${}^3_{\Lambda}\text{H}$, respectively.

A.4 Systematic uncertainties

The centrality-uncorrelated systematic uncertainty on the yield ratio is obtained as the variance of multiple reanalyses done by varying the tracking and PID selections for π , p, ${}^3\text{He}$, and ${}^3\text{H}$, and of the BDT output selections for ${}^3_{\Lambda}\text{H}$ and Ω^- around their nominal values used in the analysis. The background fit function is also changed from exponential to polynomial in the invariant mass fit of ${}^3_{\Lambda}\text{H}$ and Ω^- , while the yields of ${}^3\text{He}$ and ${}^3\text{H}$ are alternatively extracted as the integral of a Gaussian fit to the $n\sigma^{\text{TPC}}$ and $n\sigma^{\text{TOF}}$ distributions, respectively. The variations are applied coherently to antiparticles and particles to allow for the cancelation of correlated contributions in the antiparticle-to-particle yield ratios. The MC statistical precision is also considered as a centrality-uncorrelated source of systematic uncertainty. The uncertainty on the material-budget description in MC simulations is correlated with centrality. It is evaluated by varying the amount of material crossed by simulated particles by its uncertainty, estimated to be $\pm 4.5\%$ [86]. The uncertainties on the measured absorption cross sections used to correct the GEANT4 ones are also propagated to the ratios. The consistency of the results obtained with opposite magnetic field polarities is assessed by repeating the measurement separately with the two configurations: a statistically significant discrepancy of about 0.4% and 0.6% due to imperfections in the MC description is observed in semicentral and central collisions, respectively. The maximum half dispersion between the opposite field polarity results is then assigned as a further centrality-correlated uncertainty. The values of the various contributions are summarised in Table A.1.

Table A.1: Relative systematic uncertainty on the average antiparticle-to-particle ratios due to the different sources considered in the analysis. Only the statistically significant contributions to systematic uncertainties are reported in the table.

Source	$\bar{\Omega}^+/\Omega^-$	π^+/π^-	\bar{p}/p	${}^3_{\Lambda}\bar{\text{H}}/{}^3_{\Lambda}\text{H}$	${}^3\bar{\text{H}}/{}^3\text{H}$	${}^3\bar{\text{He}}/{}^3\text{He}$
Candidate selection + signal extract.	0.5%	0.05%	0.05%	10%	3%	0.5%
Monte Carlo precision	0.5%	0.1%	0.1%	1%	1%	1%
Material budget	–	0.1%	0.5%	–	–	–
Absorption cross section	–	0.7%	0.5%	1%	10%	1%
Magnetic field polarity	–	0.2–0.3%	0.2–0.3%	–	–	–

A.5 Results for the antiparticle-to-particle ratios

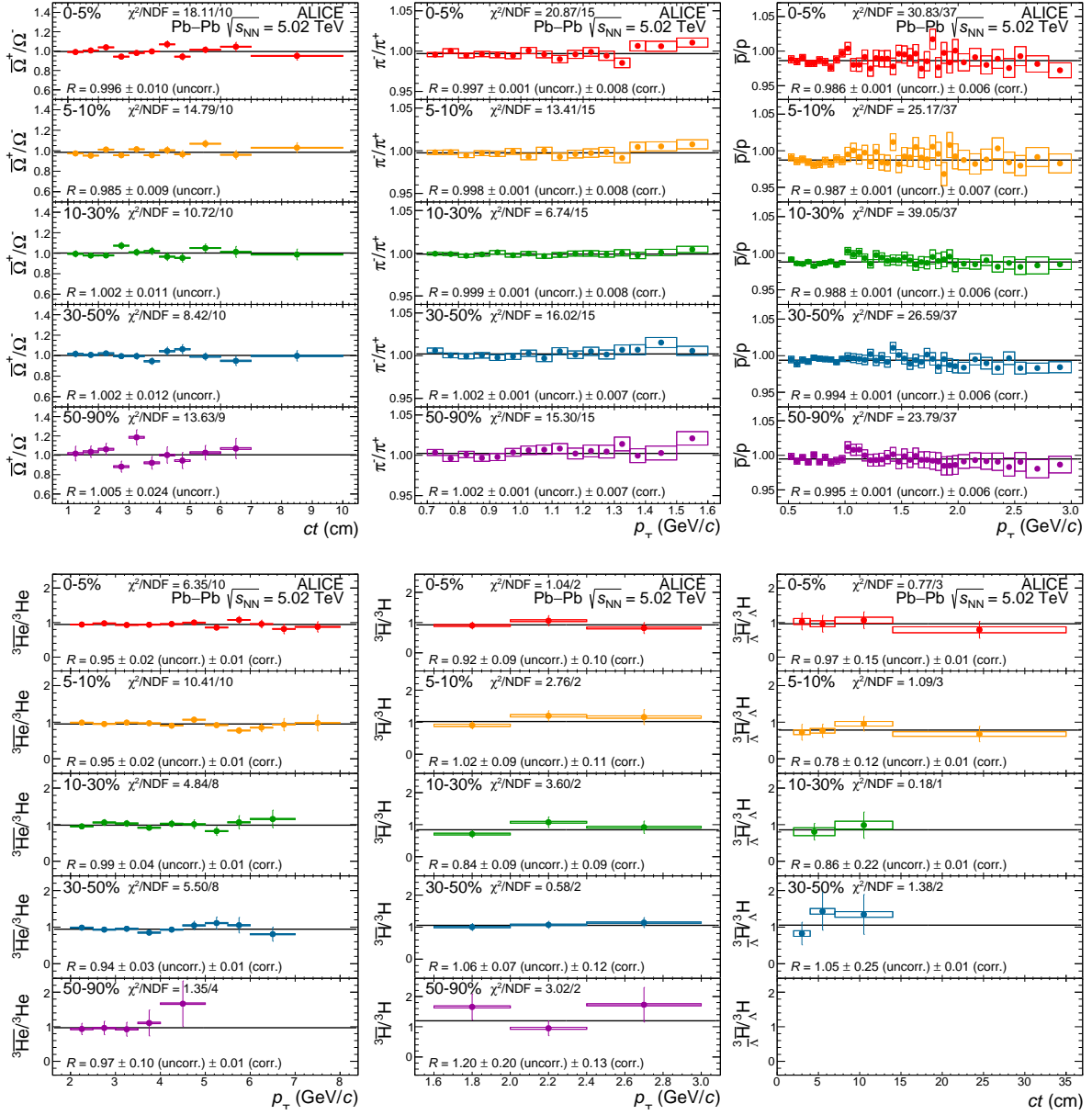


Figure A.1: p_T - and ct -differential ratios of the species used for the chemical potential measurement in the various centrality intervals. Error bars show statistical uncertainties, while boxes represent centrality-uncorrelated uncertainties. The value of R represents the averages weighted with the total uncorrelated uncertainties of the differential measurements. The correlated uncertainties are not shown in the plots.

B Covariance matrices

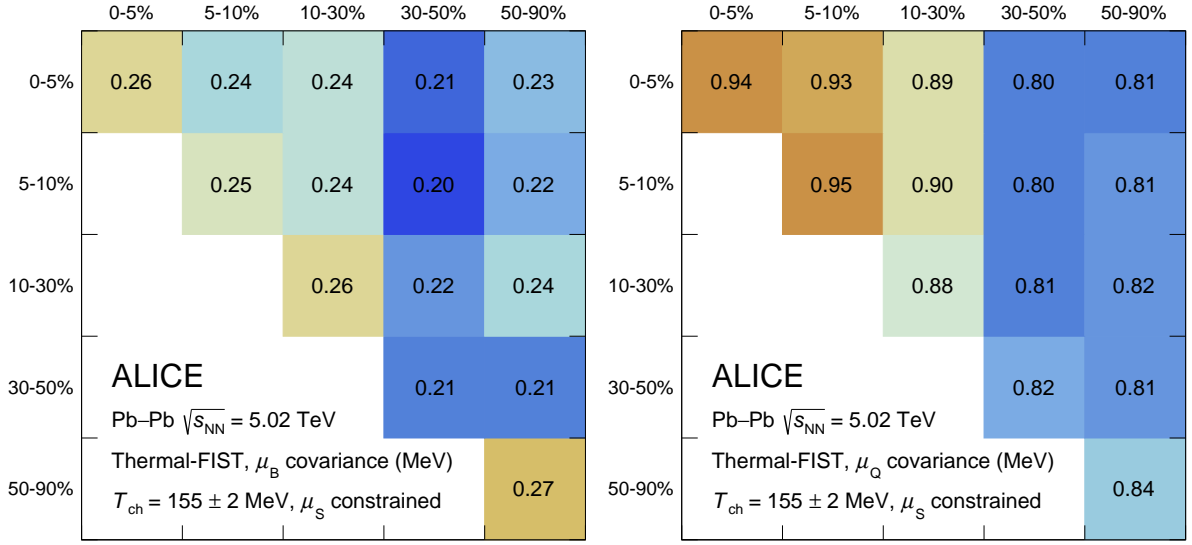


Figure B.1: Covariance matrices of μ_B (left) and μ_Q (right) obtained with Thermal-FIST [22] in the different centrality intervals.

C χ^2 profiles of chemical potential fits

C.1 Thermal-FIST model

Table C.1: Confidence intervals (C.I.) at 1σ , 2σ , and 3σ levels for μ_B and μ_Q .

Observable	1σ C.I. (MeV)	2σ C.I. (MeV)	3σ C.I. (MeV)
μ_B	[0.26, 1.16]	[-0.20, 1.61]	[-0.65, 2.07]
μ_Q	[-1.08, 0.73]	[-1.98, 1.63]	[-2.89, 2.54]

C.2 GSI-Heidelberg model

Table C.2: Confidence intervals (C.I.) at 1σ , 2σ , and 3σ levels for μ_B and μ_Q .

Observable	1σ C.I. (MeV)	2σ C.I. (MeV)	3σ C.I. (MeV)
μ_B	[0.47, 1.33]	[0.05, 1.75]	[-0.38, 2.18]

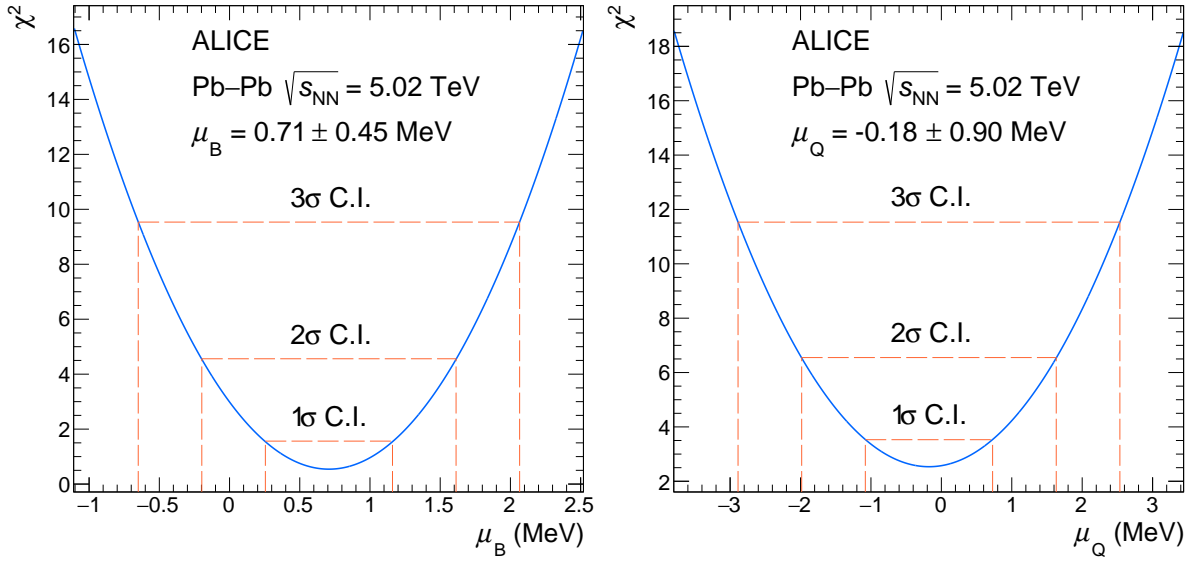


Figure C.1: Profiles of the χ^2 variable minimized in the fit of μ_B (left) and μ_Q (right) obtained with the Thermal-FIST model [22]. The values obtained from the minimization, as well as the 1 σ , 2 σ , and 3 σ confidence intervals, are reported in the figures.

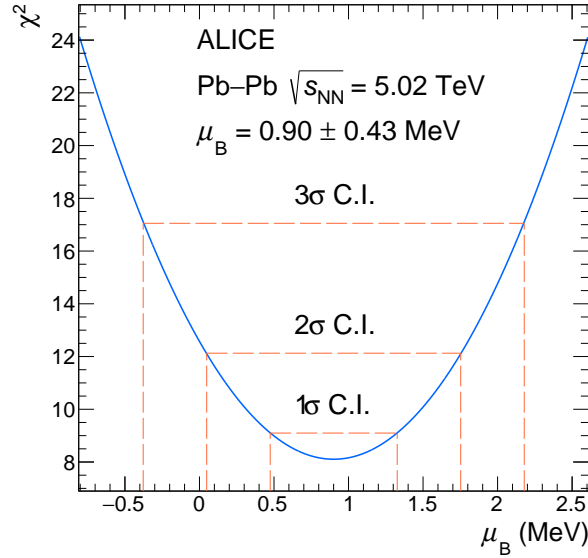


Figure C.2: Profiles of the χ^2 variable minimized in the fit of μ_B obtained with the GSI-Heidelberg model [15, 37, 76]. The values obtained from the minimization, as well as the 1 σ , 2 σ , and 3 σ confidence intervals, are reported in the figures.

D The ALICE Collaboration

S. Acharya ¹²⁸, D. Adamová ⁸⁷, G. Aglieri Rinella ³³, L. Aglietta ²⁵, M. Agnello ³⁰, N. Agrawal ²⁶, Z. Ahammed ¹³⁶, S. Ahmad ¹⁶, S.U. Ahn ⁷², I. Ahuja ³⁸, A. Akindinov ¹⁴², M. Al-Turany ⁹⁸, D. Aleksandrov ¹⁴², B. Alessandro ⁵⁷, H.M. Alfanda ⁶, R. Alfaro Molina ⁶⁸, B. Ali ¹⁶, A. Alici ²⁶, N. Alizadehvandchali ¹¹⁷, A. Alkin ³³, J. Alme ²¹, G. Alocco ⁵³, T. Alt ⁶⁵, A.R. Altamura ⁵¹, I. Altsybeev ⁹⁶, J.R. Alvarado ⁴⁵, M.N. Anaam ⁶, C. Andrei ⁴⁶, N. Andreou ¹¹⁶, A. Andronic ¹²⁷, E. Andronov ¹⁴², V. Anguelov ⁹⁵, F. Antinori ⁵⁵, P. Antonioli ⁵², N. Apadula ⁷⁵, L. Aphecetche ¹⁰⁴, H. Appelshäuser ⁶⁵, C. Arata ⁷⁴, S. Arcelli ²⁶, M. Aresti ²³, R. Arnaldi ⁵⁷, J.G.M.C.A. Arneiro ¹¹¹, I.C. Arsene ²⁰, M. Arslandok ¹³⁹, A. Augustinus ³³, R. Averbeck ⁹⁸, M.D. Azmi ¹⁶, H. Baba ¹²⁵, A. Badalà ⁵⁴, J. Bae ¹⁰⁵, Y.W. Baek ⁴¹, X. Bai ¹²¹, R. Bailhache ⁶⁵, Y. Bailung ⁴⁹, R. Bala ⁹², A. Balbino ³⁰, A. Baldisseri ¹³¹, B. Balis ², D. Banerjee ⁴, Z. Banoo ⁹², F. Barile ³², L. Barioglio ⁵⁷, M. Barlou ⁷⁹, B. Barman ⁴², G.G. Barnaföldi ⁴⁷, L.S. Barnby ⁸⁶, E. Barreau ¹⁰⁴, V. Barret ¹²⁸, L. Barreto ¹¹¹, C. Bartels ¹²⁰, K. Barth ³³, E. Bartsch ⁶⁵, N. Bastid ¹²⁸, S. Basu ⁷⁶, G. Batigne ¹⁰⁴, D. Battistini ⁹⁶, B. Batyunya ¹⁴³, D. Bauri ⁴⁸, J.L. Bazo Alba ¹⁰², I.G. Bearden ⁸⁴, C. Beattie ¹³⁹, P. Becht ⁹⁸, D. Behera ⁴⁹, I. Belikov ¹³⁰, A.D.C. Bell Hechavarria ¹²⁷, F. Bellini ²⁶, R. Bellwied ¹¹⁷, S. Belokurova ¹⁴², L.G.E. Beltran ¹¹⁰, Y.A.V. Beltran ⁴⁵, G. Bencedi ⁴⁷, S. Beole ²⁵, Y. Berdnikov ¹⁴², A. Berdnikova ⁹⁵, L. Bergmann ⁹⁵, M.G. Besoiu ⁶⁴, L. Betev ³³, P.P. Bhaduri ¹³⁶, A. Bhasin ⁹², M.A. Bhat ⁴, B. Bhattacharjee ⁴², L. Bianchi ²⁵, N. Bianchi ⁵⁰, J. Bielčik ³⁶, J. Bielčiková ⁸⁷, A.P. Bigot ¹³⁰, A. Bilandzic ⁹⁶, G. Biro ⁴⁷, S. Biswas ⁴, N. Bize ¹⁰⁴, J.T. Blair ¹⁰⁹, D. Blau ¹⁴², M.B. Blidaru ⁹⁸, N. Bluhme ³⁹, C. Blume ⁶⁵, G. Boca ^{22,56}, F. Bock ⁸⁸, T. Bodova ²¹, S. Boi ²³, J. Bok ¹⁷, L. Boldizsár ⁴⁷, M. Bombara ³⁸, P.M. Bond ³³, G. Bonomi ^{135,56}, H. Borel ¹³¹, A. Borissov ¹⁴², A.G. Borquez Carcamo ⁹⁵, H. Bossi ¹³⁹, E. Botta ²⁵, Y.E.M. Bouziani ⁶⁵, L. Bratrud ⁶⁵, P. Braun-Munzinger ⁹⁸, M. Bregant ¹¹¹, M. Broz ³⁶, G.E. Bruno ^{97,32}, M.D. Buckland ²⁴, D. Budnikov ¹⁴², H. Buesching ⁶⁵, S. Bufalino ³⁰, P. Buhler ¹⁰³, N. Burmasov ¹⁴², Z. Buthelezi ^{69,124}, A. Bylinkin ²¹, S.A. Bysiak ¹⁰⁸, J.C. Cabanillas Noris ¹¹⁰, M. Cai ⁶, H. Caines ¹³⁹, A. Caliva ²⁹, E. Calvo Villar ¹⁰², J.M.M. Camacho ¹¹⁰, P. Camerini ²⁴, F.D.M. Canedo ¹¹¹, S.L. Cantway ¹³⁹, M. Carabas ¹¹⁴, A.A. Carballo ³³, F. Carnesecchi ³³, R. Caron ¹²⁹, L.A.D. Carvalho ¹¹¹, J. Castillo Castellanos ¹³¹, F. Catalano ^{33,25}, S. Cattaruzzi ²⁴, C. Ceballos Sanchez ¹⁴³, R. Cerri ²⁵, I. Chakaberia ⁷⁵, P. Chakraborty ⁴⁸, S. Chandra ¹³⁶, S. Chapeland ³³, M. Chartier ¹²⁰, S. Chattopadhyay ¹³⁶, S. Chattopadhyay ¹⁰⁰, T. Cheng ^{98,6}, C. Cheshkov ¹²⁹, V. Chibante Barroso ³³, D.D. Chinellato ¹¹², E.S. Chizzali ^{11,96}, J. Cho ⁵⁹, S. Cho ⁵⁹, P. Chochula ³³, D. Choudhury ⁴², P. Christakoglou ⁸⁵, C.H. Christensen ⁸⁴, P. Christiansen ⁷⁶, T. Chujo ¹²⁶, M. Ciacco ³⁰, C. Cicalo ⁵³, M.R. Ciupek ⁹⁸, G. Clai ^{III,52}, F. Colamaria ⁵¹, J.S. Colburn ¹⁰¹, D. Colella ^{97,32}, M. Colocci ²⁶, M. Concas ³³, G. Conesa Balbastre ⁷⁴, Z. Conesa del Valle ¹³², G. Contin ²⁴, J.G. Contreras ³⁶, M.L. Coquet ¹³¹, P. Cortese ^{134,57}, M.R. Cosentino ¹¹³, F. Costa ³³, S. Costanza ^{22,56}, C. Cot ¹³², J. Crkovská ⁹⁵, P. Crochet ¹²⁸, R. Cruz-Torres ⁷⁵, P. Cui ⁶, A. Dainese ⁵⁵, M.C. Danisch ⁹⁵, A. Danu ⁶⁴, P. Das ⁸¹, P. Das ⁴, S. Das ⁴, A.R. Dash ¹²⁷, S. Dash ⁴⁸, A. De Caro ²⁹, G. de Cataldo ⁵¹, J. de Cuveland ³⁹, A. De Falco ²³, D. De Gruttola ²⁹, N. De Marco ⁵⁷, C. De Martin ²⁴, S. De Pasquale ²⁹, R. Deb ¹³⁵, R. Del Grande ⁹⁶, L. Dello Stritto ^{33,29}, W. Deng ⁶, P. Dhankher ¹⁹, D. Di Bari ³², A. Di Mauro ³³, B. Diab ¹³¹, R.A. Diaz ^{143,7}, T. Dietel ¹¹⁵, Y. Ding ⁶, J. Ditzel ⁶⁵, R. Divià ³³, D.U. Dixit ¹⁹, Ø. Djuvsland ²¹, U. Dmitrieva ¹⁴², A. Dobrin ⁶⁴, B. Dönigus ⁶⁵, J.M. Dubinski ¹³⁷, A. Dubla ⁹⁸, S. Dudi ⁹¹, P. Dupieux ¹²⁸, M. Durkac ¹⁰⁷, N. Dzalaiova ¹³, T.M. Eder ¹²⁷, R.J. Ehlers ⁷⁵, F. Eisenhut ⁶⁵, R. Ejima ⁹³, D. Elia ⁵¹, B. Erasmus ¹⁰⁴, F. Ercolessi ²⁶, B. Espagnon ¹³², G. Eulisse ³³, D. Evans ¹⁰¹, S. Evdokimov ¹⁴², L. Fabbietti ⁹⁶, M. Faggin ²⁸, J. Faivre ⁷⁴, F. Fan ⁶, W. Fan ⁷⁵, A. Fantoni ⁵⁰, M. Fasel ⁸⁸, A. Feliciello ⁵⁷, G. Feofilov ¹⁴², A. Fernández Téllez ⁴⁵, L. Ferrandi ¹¹¹, M.B. Ferrer ³³, A. Ferrero ¹³¹, C. Ferrero ^{IV,57}, A. Ferretti ²⁵, V.J.G. Feuillard ⁹⁵, V. Filova ³⁶, D. Finogeev ¹⁴², F.M. Fionda ⁵³, E. Flatland ³³, F. Flor ¹¹⁷, A.N. Flores ¹⁰⁹, S. Foertsch ⁶⁹, I. Fokin ⁹⁵, S. Fokin ¹⁴², E. Fragiaco ⁵⁸, E. Frajna ⁴⁷, U. Fuchs ³³, N. Funicello ²⁹, C. Furget ⁷⁴, A. Furs ¹⁴², T. Fusayasu ⁹⁹, J.J. Gaardhøje ⁸⁴, M. Gagliardi ²⁵, A.M. Gago ¹⁰², T. Gahlaut ⁴⁸, C.D. Galvan ¹¹⁰, D.R. Gangadharan ¹¹⁷, P. Ganoti ⁷⁹, C. Garabatos ⁹⁸, T. García Chávez ⁴⁵, E. García-Solis ⁹, C. Gargiulo ³³, P. Gasik ⁹⁸, A. Gautam ¹¹⁹, M.B. Gay Ducati ⁶⁷, M. Germain ¹⁰⁴, A. Ghimouz ¹²⁶, C. Ghosh ¹³⁶, M. Giacalone ⁵², G. Gioachin ³⁰, P. Giubellino ^{98,57}, P. Giubilato ²⁸, A.M.C. Glaenger ¹³¹, P. Glässel ⁹⁵, E. Glimos ¹²³, D.J.Q. Goh ⁷⁷, V. Gonzalez ¹³⁸, P. Gordeev ¹⁴², M. Gorgon ², K. Goswami ⁴⁹, S. Gotovac ³⁴, V. Grabski ⁶⁸, L.K. Graczykowski ¹³⁷, E. Grecka ⁸⁷, A. Grelli ⁶⁰, C. Grigoras ³³, V. Grigoriev ¹⁴², S. Grigoryan ^{143,1}, F. Grosa ³³, J.F. Grosse-Oetringhaus ³³, R. Grosso ⁹⁸, D. Grund ³⁶, N.A. Grunwald ⁹⁵, G.G. Guardiani ¹¹², R. Guernane ⁷⁴, M. Guilbaud ¹⁰⁴, K. Gulbrandsen ⁸⁴, T. Gündem ⁶⁵, T. Gunji ¹²⁵,

W. Guo⁶, A. Gupta⁹², R. Gupta⁹², R. Gupta⁴⁹, K. Gwizdziel¹³⁷, L. Gyulai⁴⁷, C. Hadjidakis¹³², F.U. Haider⁹², S. Haidlova³⁶, M. Haldar⁴, H. Hamagaki⁷⁷, A. Hamdi⁷⁵, Y. Han¹⁴⁰, B.G. Hanley¹³⁸, R. Hannigan¹⁰⁹, J. Hansen⁷⁶, J.W. Harris¹³⁹, A. Harton⁹, M.V. Hartung⁶⁵, H. Hassan¹¹⁸, D. Hatzifotiadou⁵², P. Hauer⁴³, L.B. Havener¹³⁹, E. Hellbär⁹⁸, H. Helstrup³⁵, M. Hemmer⁶⁵, T. Herman³⁶, G. Herrera Corral⁸, F. Herrmann¹²⁷, S. Herrmann¹²⁹, K.F. Hetland³⁵, B. Heybeck⁶⁵, H. Hillemanns³³, B. Hippolyte¹³⁰, F.W. Hoffmann⁷¹, B. Hofman⁶⁰, G.H. Hong¹⁴⁰, M. Horst⁹⁶, A. Horzyk², Y. Hou⁶, P. Hristov³³, P. Huhn⁶⁵, L.M. Huhta¹¹⁸, T.J. Humanic⁸⁹, A. Hutson¹¹⁷, D. Hutter³⁹, M.C. Hwang¹⁹, R. Ilkaev¹⁴², H. Ilyas¹⁴, M. Inaba¹²⁶, G.M. Innocenti³³, M. Ippolitov¹⁴², A. Isakov⁸⁵, T. Isidori¹¹⁹, M.S. Islam¹⁰⁰, M. Ivanov⁹⁸, M. Ivanov¹³, V. Ivanov¹⁴², K.E. Iversen⁷⁶, M. Jablonski², B. Jacak^{19,75}, N. Jacazio²⁶, P.M. Jacobs⁷⁵, S. Jadlovská¹⁰⁷, J. Jadlovský¹⁰⁷, S. Jaelani⁸³, C. Jahnke¹¹¹, M.J. Jakubowska¹³⁷, M.A. Janik¹³⁷, T. Janson⁷¹, S. Ji¹⁷, S. Jia¹⁰, A.A.P. Jimenez⁶⁶, F. Jonas^{75,88,127}, D.M. Jones¹²⁰, J.M. Jowett^{33,98}, J. Jung⁶⁵, M. Jung⁶⁵, A. Junique³³, A. Jusko¹⁰¹, J. Kaewjai¹⁰⁶, P. Kalinak⁶¹, A.S. Kalteyer⁹⁸, A. Kalweit³³, A. Karasu Uysal⁷³, D. Karatovic⁹⁰, O. Karavichev¹⁴², T. Karavicheva¹⁴², P. Karczmarczyk¹³⁷, E. Karpechev¹⁴², M.J. Karwowska^{33,137}, U. Keschull⁷¹, R. Keidel¹⁴¹, D.L.D. Keijdener⁶⁰, M. Keil³³, B. Ketzer⁴³, S.S. Khade⁴⁹, A.M. Khan¹²¹, S. Khan¹⁶, A. Khanzadeev¹⁴², Y. Kharlov¹⁴², A. Khatun¹¹⁹, A. Khuntia³⁶, Z. Khuranova⁶⁵, B. Kileng³⁵, B. Kim¹⁰⁵, C. Kim¹⁷, D.J. Kim¹¹⁸, E.J. Kim⁷⁰, J. Kim¹⁴⁰, J. Kim⁵⁹, J. Kim⁷⁰, M. Kim¹⁹, S. Kim¹⁸, T. Kim¹⁴⁰, K. Kimura⁹³, S. Kirsch⁶⁵, I. Kisel³⁹, S. Kiselev¹⁴², A. Kisiel¹³⁷, J.P. Kitowski², J.L. Klay⁵, J. Klein³³, S. Klein⁷⁵, C. Klein-Bösing¹²⁷, M. Kleiner⁶⁵, T. Klemenz⁹⁶, A. Kluge³³, C. Kobdaj¹⁰⁶, T. Kollegger⁹⁸, A. Kondratyev¹⁴³, N. Kondratyeva¹⁴², J. König⁶⁵, S.A. Königstorfer⁹⁶, P.J. Konopka³³, G. Kornakov¹³⁷, M. Korwieser⁹⁶, S.D. Koryciak², A. Kotliarov⁸⁷, N. Kovacic⁹⁰, V. Kovalenko¹⁴², M. Kowalski¹⁰⁸, V. Kozuharov³⁷, I. Králik⁶¹, A. Kravčáková³⁸, L. Krcal^{33,39}, M. Krivda^{101,61}, F. Krizek⁸⁷, K. Krizkova Gajdosova³³, M. Kroesen⁹⁵, M. Krüger⁶⁵, D.M. Krupova³⁶, E. Kryshen¹⁴², V. Kučera⁵⁹, C. Kuhn¹³⁰, P.G. Kuijer⁸⁵, T. Kumaoka¹²⁶, D. Kumar¹³⁶, L. Kumar⁹¹, N. Kumar⁹¹, S. Kumar³², S. Kundu³³, P. Kurashvili⁸⁰, A. Kurepin¹⁴², A.B. Kurepin¹⁴², A. Kuryakin¹⁴², S. Kushpil⁸⁷, V. Kuskov¹⁴², M. Kutyla¹³⁷, M.J. Kweon⁵⁹, Y. Kwon¹⁴⁰, S.L. La Pointe³⁹, P. La Rocca²⁷, A. Lakrathok¹⁰⁶, M. Lamanna³³, A.R. Landou⁷⁴, R. Langoy¹²², P. Larionov³³, E. Laudi³³, L. Lautner^{33,96}, R. Lavicka¹⁰³, R. Lea^{135,56}, H. Lee¹⁰⁵, I. Legrand⁴⁶, G. Legras¹²⁷, J. Lehrbach³⁹, T.M. Lelek², R.C. Lemmon⁸⁶, I. León Monzón¹¹⁰, M.M. Lesch⁹⁶, E.D. Lesser¹⁹, P. Lévai⁴⁷, X. Li¹⁰, B.E. Liang-gilman¹⁹, J. Lien¹²², R. Lietava¹⁰¹, I. Likmeta¹¹⁷, B. Lim²⁵, S.H. Lim¹⁷, V. Lindenstruth³⁹, A. Lindner⁴⁶, C. Lippmann⁹⁸, D.H. Liu⁶, J. Liu¹²⁰, G.S.S. Liveraro¹¹², I.M. Lofnes²¹, C. Loizides⁸⁸, S. Lokos¹⁰⁸, J. Lömker⁶⁰, P. Loncar³⁴, X. Lopez¹²⁸, E. López Torres⁷, P. Lu^{98,121}, F.V. Lugo⁶⁸, J.R. Luhder¹²⁷, M. Lunardon²⁸, G. Luparello⁵⁸, Y.G. Ma⁴⁰, M. Mager³³, A. Maire¹³⁰, E.M. Majerz², M.V. Makariev³⁷, M. Malaev¹⁴², G. Malfattore²⁶, N.M. Malik⁹², Q.W. Malik²⁰, S.K. Malik⁹², L. Malinina^{I,VIII,143}, D. Mallick¹³², N. Mallick⁴⁹, G. Mandaglio^{31,54}, S.K. Mandal⁸⁰, V. Manko¹⁴², F. Manso¹²⁸, V. Manzari⁵¹, Y. Mao⁶, R.W. Marcjan², G.V. Margagliotti²⁴, A. Margotti⁵², A. Marín⁹⁸, C. Markert¹⁰⁹, P. Martinengo³³, M.I. Martínez⁴⁵, G. Martínez García¹⁰⁴, M.P.P. Martins¹¹¹, S. Masciocchi⁹⁸, M. Masera²⁵, A. Masoni⁵³, L. Massacrier¹³², O. Massen⁶⁰, A. Mastroserio^{133,51}, O. Matonoha⁷⁶, S. Mattiazzo²⁸, A. Matyja¹⁰⁸, C. Mayer¹⁰⁸, A.L. Mazuecos³³, F. Mazzaschi²⁵, M. Mazzilli³³, J.E. Mdhuli¹²⁴, Y. Melikyan⁴⁴, A. Menchaca-Rocha⁶⁸, J.E.M. Mendez⁶⁶, E. Meninno¹⁰³, A.S. Menon¹¹⁷, M. Meres¹³, Y. Miake¹²⁶, L. Micheletti³³, D.L. Mihaylov⁹⁶, K. Mikhaylov^{143,142}, D. Miśkowiec⁹⁸, A. Modak⁴, B. Mohanty⁸¹, M. Mohisin Khan^{VI,16}, M.A. Molander⁴⁴, S. Monira¹³⁷, C. Mordasini¹¹⁸, D.A. Moreira De Godoy¹²⁷, I. Morozov¹⁴², A. Morsch³³, T. Mrnjavac³³, V. Muccifora⁵⁰, S. Muhuri¹³⁶, J.D. Mulligan⁷⁵, A. Mulliri²³, M.G. Munhoz¹¹¹, R.H. Munzer⁶⁵, H. Murakami¹²⁵, S. Murray¹¹⁵, L. Musa³³, J. Musinsky⁶¹, J.W. Myrcha¹³⁷, B. Naik¹²⁴, A.I. Nambrath¹⁹, B.K. Nandi⁴⁸, R. Nania⁵², E. Nappi⁵¹, A.F. Nassirpour¹⁸, A. Nath⁹⁵, C. Nattrass¹²³, M.N. Naydenov³⁷, A. Neagu²⁰, A. Negru¹¹⁴, E. Nekrasova¹⁴², L. Nellen⁶⁶, R. Nepeivoda⁷⁶, S. Nese²⁰, G. Neskovic³⁹, N. Nicassio⁵¹, B.S. Nielsen⁸⁴, E.G. Nielsen⁸⁴, S. Nikolaev¹⁴², S. Nikulin¹⁴², V. Nikulin¹⁴², F. Noferini⁵², S. Noh¹², P. Nomokonov¹⁴³, J. Norman¹²⁰, N. Novitzky⁸⁸, P. Nowakowski¹³⁷, A. Nyanin¹⁴², J. Nystrand²¹, S. Oh¹⁸, A. Ohlson⁷⁶, V.A. Okorokov¹⁴², J. Oleniacz¹³⁷, A. Onnerstad¹¹⁸, C. Oppedisano⁵⁷, A. Ortiz Velasquez⁶⁶, J. Otwinowski¹⁰⁸, M. Oya⁹³, K. Oyama⁷⁷, Y. Pachmayer⁹⁵, S. Padhan⁴⁸, D. Pagano^{135,56}, G. Paić⁶⁶, S. Paisano-Guzmán⁴⁵, A. Palasciano⁵¹, S. Panebianco¹³¹, H. Park¹²⁶, H. Park¹⁰⁵, J. Park⁵⁹, J.E. Parkkila³³, Y. Patley⁴⁸, B. Paul²³,

M.M.D.M. Paulino¹¹¹, H. Pei⁶, T. Peitzmann⁶⁰, X. Peng¹¹, M. Pennisi²⁵, S. Perciballi²⁵, D. Peresunko¹⁴², G.M. Perez⁷, Y. Pestov¹⁴², V. Petrov¹⁴², M. Petrovici⁴⁶, R.P. Pezzi^{104,67}, S. Piano⁵⁸, M. Pikna¹³, P. Pillot¹⁰⁴, O. Pinazza^{52,33}, L. Pinsky¹¹⁷, C. Pinto⁹⁶, S. Pisano⁵⁰, M. Płoskoń⁷⁵, M. Planinic⁹⁰, F. Pliquett⁶⁵, M.G. Poghosyan⁸⁸, B. Polichtchouk¹⁴², S. Politano³⁰, N. Poljak⁹⁰, A. Pop⁴⁶, S. Porteboeuf-Houssais¹²⁸, V. Pozdniakov¹⁴³, I.Y. Pozos⁴⁵, K.K. Pradhan⁴⁹, S.K. Prasad⁴, S. Prasad⁴⁹, R. Preghenella⁵², F. Prino⁵⁷, C.A. Pruneau¹³⁸, I. Pshenichnov¹⁴², M. Puccio³³, S. Pucillo²⁵, Z. Pugelova¹⁰⁷, S. Qiu⁸⁵, L. Quaglia²⁵, S. Ragoni¹⁵, A. Rai¹³⁹, A. Rakotozafindrabe¹³¹, L. Ramello^{134,57}, F. Rami¹³⁰, T.A. Rancien⁷⁴, M. Rasa²⁷, S.S. Räsänen⁴⁴, R. Rath⁵², M.P. Rauch²¹, I. Ravasenga³³, K.F. Read^{88,123}, C. Reckziegel¹¹³, A.R. Redelbach³⁹, K. Redlich^{VII,80}, C.A. Reetz⁹⁸, H.D. Regules-Medel⁴⁵, A. Rehman²¹, F. Reidt³³, H.A. Reme-Ness³⁵, Z. Rescakova³⁸, K. Reygers⁹⁵, A. Riabov¹⁴², V. Riabov¹⁴², R. Ricci²⁹, M. Richter²⁰, A.A. Riedel⁹⁶, W. Riegler³³, A.G. Riffero²⁵, C. Ristea⁶⁴, M.V. Rodriguez³³, M. Rodríguez Cahuantzi⁴⁵, S.A. Rodríguez Ramírez⁴⁵, K. Røed²⁰, R. Rogalev¹⁴², E. Rogochaya¹⁴³, T.S. Rogoschinski⁶⁵, D. Rohr³³, D. Röhrich²¹, P.F. Rojas⁴⁵, S. Rojas Torres³⁶, P.S. Rokita¹³⁷, G. Romanenko²⁶, F. Ronchetti⁵⁰, A. Rosano^{31,54}, E.D. Rosas⁶⁶, K. Roslon¹³⁷, A. Rossi⁵⁵, A. Roy⁴⁹, S. Roy⁴⁸, N. Rubini²⁶, D. Ruggiano¹³⁷, R. Rui²⁴, P.G. Russek², R. Russo⁸⁵, A. Rustamov⁸², E. Ryabinkin¹⁴², Y. Ryabov¹⁴², A. Rybicki¹⁰⁸, H. Rytönen¹¹⁸, J. Ryu¹⁷, W. Rzesza¹³⁷, O.A.M. Saarimäki⁴⁴, S. Sadhu³², S. Sadosky¹⁴², J. Saetre²¹, K. Šafařík³⁶, P. Saha⁴², S.K. Saha⁴, S. Saha⁸¹, B. Sahoo⁴⁹, R. Sahoo⁴⁹, S. Sahoo⁶², D. Sahu⁴⁹, P.K. Sahu⁶², J. Saini¹³⁶, K. Sajdakova³⁸, S. Sakai¹²⁶, M.P. Salvan⁹⁸, S. Sambyal⁹², D. Samitz¹⁰³, I. Sanna^{33,96}, T.B. Saramela¹¹¹, D. Sarkar⁸⁴, P. Sarma⁴², V. Sarritzu²³, V.M. Sarti⁹⁶, M.H.P. Sas³³, S. Sawan⁸¹, E. Scapparone⁵², J. Schambach⁸⁸, H.S. Scheid⁶⁵, C. Schiaua⁴⁶, R. Schicker⁹⁵, F. Schlepfer⁹⁵, A. Schmah⁹⁸, C. Schmidt⁹⁸, H.R. Schmidt⁹⁴, M.O. Schmidt³³, M. Schmidt⁹⁴, N.V. Schmidt⁸⁸, A.R. Schmier¹²³, R. Schotter¹³⁰, A. Schröter³⁹, J. Schukraft³³, K. Schweda⁹⁸, G. Scioli²⁶, E. Scomparin⁵⁷, J.E. Seger¹⁵, Y. Sekiguchi¹²⁵, D. Sekihata¹²⁵, M. Selina⁸⁵, I. Selyuzhenkov⁹⁸, S. Senyukov¹³⁰, J.J. Seo⁹⁵, D. Serebryakov¹⁴², L. Serkin⁶⁶, L. Šerkšnytė⁹⁶, A. Sevcenco⁶⁴, T.J. Shaba⁶⁹, A. Shabetai¹⁰⁴, R. Shahoyan³³, A. Shangaraev¹⁴², B. Sharma⁹², D. Sharma⁴⁸, H. Sharma⁵⁵, M. Sharma⁹², S. Sharma⁷⁷, S. Sharma⁹², U. Sharma⁹², A. Shatat¹³², O. Sheibani¹¹⁷, K. Shigaki⁹³, M. Shimomura⁷⁸, J. Shin¹², S. Shirinkin¹⁴², Q. Shou⁴⁰, Y. Sibiriak¹⁴², S. Siddhanta⁵³, T. Siemiarczuk⁸⁰, T.F. Silva¹¹¹, D. Silvermyr⁷⁶, T. Simantathammakul¹⁰⁶, R. Simeonov³⁷, B. Singh⁹², B. Singh⁹⁶, K. Singh⁴⁹, R. Singh⁸¹, R. Singh⁹², R. Singh^{98,49}, S. Singh¹⁶, V.K. Singh¹³⁶, V. Singhal¹³⁶, T. Sinha¹⁰⁰, B. Sitar¹³, M. Sitta^{134,57}, T.B. Skaali²⁰, G. Skorodumovs⁹⁵, M. Slupecki⁴⁴, N. Smirnov¹³⁹, R.J.M. Snellings⁶⁰, E.H. Solheim²⁰, J. Song¹⁷, C. Sonnabend^{33,98}, J.M. Sonneveld⁸⁵, F. Soramel²⁸, A.B. Soto-hernandez⁸⁹, R. Spijkers⁸⁵, I. Sputowska¹⁰⁸, J. Staa⁷⁶, J. Stachel⁹⁵, I. Stan⁶⁴, P.J. Steffanic¹²³, S.F. Stiefelmaier⁹⁵, D. Stocco¹⁰⁴, I. Storehaug²⁰, P. Stratmann¹²⁷, S. Strazzi²⁶, A. Sturmiolo^{31,54}, C.P. Stylianidis⁸⁵, A.A.P. Suaide¹¹¹, C. Suire¹³², M. Sukhanov¹⁴², M. Suljic³³, R. Sultanov¹⁴², V. Sumberia⁹², S. Sumowidagdo⁸³, I. Szarka¹³, M. Szymkowski¹³⁷, S.F. Taghavi⁹⁶, G. Taillepied⁹⁸, J. Takahashi¹¹², G.J. Tambave⁸¹, S. Tang⁶, Z. Tang¹²¹, J.D. Tapia Takaki¹¹⁹, N. Tapus¹¹⁴, L.A. Tarasovicova¹²⁷, M.G. Tazila⁴⁶, G.F. Tassielli³², A. Tauro³³, A. Tavira García¹³², G. Tejeda Muñoz⁴⁵, A. Telesca³³, L. Terlizzi²⁵, C. Terrevoli¹¹⁷, S. Thakur⁴, D. Thomas¹⁰⁹, A. Tikhonov¹⁴², N. Tiltmann^{33,127}, A.R. Timmins¹¹⁷, M. Tkacik¹⁰⁷, T. Tkacik¹⁰⁷, A. Toia⁶⁵, R. Tokumoto⁹³, K. Tomohiro⁹³, N. Topilskaya¹⁴², M. Toppi⁵⁰, T. Tork¹³², V.V. Torres¹⁰⁴, A.G. Torres Ramos³², A. Trifiro' ^{31,54}, A.S. Triolo^{33,31,54}, S. Tripathy⁵², T. Tripathy⁴⁸, S. Trogolo³³, V. Trubnikov³, W.H. Trzaska¹¹⁸, T.P. Trzcinski¹³⁷, A. Tumkin¹⁴², R. Turrisi⁵⁵, T.S. Tveter²⁰, K. Ullaland²¹, B. Ulukutlu⁹⁶, A. Uras¹²⁹, M. Urioni¹³⁵, G.L. Usai²³, M. Vala³⁸, N. Valle²², L.V.R. van Doremalen⁶⁰, M. van Leeuwen⁸⁵, C.A. van Veen⁹⁵, R.J.G. van Weelden⁸⁵, P. Vande Vyvre³³, D. Varga⁴⁷, Z. Varga⁴⁷, P. Vargas Torres⁶⁶, M. Vasileiou⁷⁹, A. Vasiliev¹⁴², O. Vázquez Doce⁵⁰, O. Vazquez Rueda¹¹⁷, V. Vechernin¹⁴², E. Vercellin²⁵, S. Vergara Limón⁴⁵, R. Verma⁴⁸, L. Vermunt⁹⁸, R. Vértesi⁴⁷, M. Verweij⁶⁰, L. Vickovic³⁴, Z. Vilakazi¹²⁴, O. Villalobos Baillie¹⁰¹, A. Villani²⁴, A. Vinogradov¹⁴², T. Virgili²⁹, M.M.O. Virta¹¹⁸, V. Vislavicius⁷⁶, A. Vodopyanov¹⁴³, B. Volkel³³, M.A. Völkl⁹⁵, S.A. Voloshin¹³⁸, G. Volpe³², B. von Haller³³, I. Vorobyev³³, N. Vozniuk¹⁴², J. Vrláková³⁸, J. Wan⁴⁰, C. Wang⁴⁰, D. Wang⁴⁰, Y. Wang⁴⁰, Y. Wang⁶, A. Wegrzynek³³, F.T. Weiglhofer³⁹, S.C. Wenzel³³, J.P. Wessels¹²⁷, J. Wiechula⁶⁵, J. Wikne²⁰, G. Wilk⁸⁰, J. Wilkinson⁹⁸, G.A. Willems¹²⁷, B. Windelband⁹⁵, M. Winn¹³¹, J.R. Wright¹⁰⁹, W. Wu⁴⁰, Y. Wu¹²¹, Z. Xiong¹²¹, R. Xu⁶, A. Yadav⁴³, A.K. Yadav¹³⁶, S. Yalcin⁷³, Y. Yamaguchi⁹³, S. Yang²¹, S. Yano⁹³, E.R. Yeats¹⁹, Z. Yin⁶, I.-K. Yoo¹⁷, J.H. Yoon⁵⁹,

H. Yu¹², S. Yuan²¹, A. Yuncu⁹⁵, V. Zaccaro²⁴, C. Zampolli³³, F. Zanone⁹⁵, N. Zardoshti³³,
 A. Zarochentsev¹⁴², P. Závada⁶³, N. Zaviyalov¹⁴², M. Zhalov¹⁴², B. Zhang⁶, C. Zhang¹³¹,
 L. Zhang⁴⁰, M. Zhang⁶, S. Zhang⁴⁰, X. Zhang⁶, Y. Zhang¹²¹, Z. Zhang⁶, M. Zhao¹⁰,
 V. Zhrebchevskii¹⁴², Y. Zhi¹⁰, C. Zhong⁴⁰, D. Zhou⁶, Y. Zhou⁸⁴, J. Zhu^{55,6}, Y. Zhu⁶,
 S.C. Zugeravel⁵⁷, N. Zurlo^{135,56}

Affiliation Notes

^I Deceased

^{II} Also at: Max-Planck-Institut für Physik, Munich, Germany

^{III} Also at: Italian National Agency for New Technologies, Energy and Sustainable Economic Development (ENEA), Bologna, Italy

^{IV} Also at: Dipartimento DET del Politecnico di Torino, Turin, Italy

^V Also at: Yildiz Technical University, Istanbul, Türkiye

^{VI} Also at: Department of Applied Physics, Aligarh Muslim University, Aligarh, India

^{VII} Also at: Institute of Theoretical Physics, University of Wrocław, Poland

^{VIII} Also at: An institution covered by a cooperation agreement with CERN

Collaboration Institutes

¹ A.I. Alikhanyan National Science Laboratory (Yerevan Physics Institute) Foundation, Yerevan, Armenia

² AGH University of Krakow, Cracow, Poland

³ Bogolyubov Institute for Theoretical Physics, National Academy of Sciences of Ukraine, Kiev, Ukraine

⁴ Bose Institute, Department of Physics and Centre for Astroparticle Physics and Space Science (CAPSS), Kolkata, India

⁵ California Polytechnic State University, San Luis Obispo, California, United States

⁶ Central China Normal University, Wuhan, China

⁷ Centro de Aplicaciones Tecnológicas y Desarrollo Nuclear (CEADEN), Havana, Cuba

⁸ Centro de Investigación y de Estudios Avanzados (CINVESTAV), Mexico City and Mérida, Mexico

⁹ Chicago State University, Chicago, Illinois, United States

¹⁰ China Institute of Atomic Energy, Beijing, China

¹¹ China University of Geosciences, Wuhan, China

¹² Chungbuk National University, Cheongju, Republic of Korea

¹³ Comenius University Bratislava, Faculty of Mathematics, Physics and Informatics, Bratislava, Slovak Republic

¹⁴ COMSATS University Islamabad, Islamabad, Pakistan

¹⁵ Creighton University, Omaha, Nebraska, United States

¹⁶ Department of Physics, Aligarh Muslim University, Aligarh, India

¹⁷ Department of Physics, Pusan National University, Pusan, Republic of Korea

¹⁸ Department of Physics, Sejong University, Seoul, Republic of Korea

¹⁹ Department of Physics, University of California, Berkeley, California, United States

²⁰ Department of Physics, University of Oslo, Oslo, Norway

²¹ Department of Physics and Technology, University of Bergen, Bergen, Norway

²² Dipartimento di Fisica, Università di Pavia, Pavia, Italy

²³ Dipartimento di Fisica dell'Università and Sezione INFN, Cagliari, Italy

²⁴ Dipartimento di Fisica dell'Università and Sezione INFN, Trieste, Italy

²⁵ Dipartimento di Fisica dell'Università and Sezione INFN, Turin, Italy

²⁶ Dipartimento di Fisica e Astronomia dell'Università and Sezione INFN, Bologna, Italy

²⁷ Dipartimento di Fisica e Astronomia dell'Università and Sezione INFN, Catania, Italy

²⁸ Dipartimento di Fisica e Astronomia dell'Università and Sezione INFN, Padova, Italy

²⁹ Dipartimento di Fisica 'E.R. Caianiello' dell'Università and Gruppo Collegato INFN, Salerno, Italy

³⁰ Dipartimento DISAT del Politecnico and Sezione INFN, Turin, Italy

³¹ Dipartimento di Scienze MIIFT, Università di Messina, Messina, Italy

³² Dipartimento Interateneo di Fisica 'M. Merlin' and Sezione INFN, Bari, Italy

³³ European Organization for Nuclear Research (CERN), Geneva, Switzerland

³⁴ Faculty of Electrical Engineering, Mechanical Engineering and Naval Architecture, University of Split, Split, Croatia

- ³⁵ Faculty of Engineering and Science, Western Norway University of Applied Sciences, Bergen, Norway
- ³⁶ Faculty of Nuclear Sciences and Physical Engineering, Czech Technical University in Prague, Prague, Czech Republic
- ³⁷ Faculty of Physics, Sofia University, Sofia, Bulgaria
- ³⁸ Faculty of Science, P.J. Šafárik University, Košice, Slovak Republic
- ³⁹ Frankfurt Institute for Advanced Studies, Johann Wolfgang Goethe-Universität Frankfurt, Frankfurt, Germany
- ⁴⁰ Fudan University, Shanghai, China
- ⁴¹ Gangneung-Wonju National University, Gangneung, Republic of Korea
- ⁴² Gauhati University, Department of Physics, Guwahati, India
- ⁴³ Helmholtz-Institut für Strahlen- und Kernphysik, Rheinische Friedrich-Wilhelms-Universität Bonn, Bonn, Germany
- ⁴⁴ Helsinki Institute of Physics (HIP), Helsinki, Finland
- ⁴⁵ High Energy Physics Group, Universidad Autónoma de Puebla, Puebla, Mexico
- ⁴⁶ Horia Hulubei National Institute of Physics and Nuclear Engineering, Bucharest, Romania
- ⁴⁷ HUN-REN Wigner Research Centre for Physics, Budapest, Hungary
- ⁴⁸ Indian Institute of Technology Bombay (IIT), Mumbai, India
- ⁴⁹ Indian Institute of Technology Indore, Indore, India
- ⁵⁰ INFN, Laboratori Nazionali di Frascati, Frascati, Italy
- ⁵¹ INFN, Sezione di Bari, Bari, Italy
- ⁵² INFN, Sezione di Bologna, Bologna, Italy
- ⁵³ INFN, Sezione di Cagliari, Cagliari, Italy
- ⁵⁴ INFN, Sezione di Catania, Catania, Italy
- ⁵⁵ INFN, Sezione di Padova, Padova, Italy
- ⁵⁶ INFN, Sezione di Pavia, Pavia, Italy
- ⁵⁷ INFN, Sezione di Torino, Turin, Italy
- ⁵⁸ INFN, Sezione di Trieste, Trieste, Italy
- ⁵⁹ Inha University, Incheon, Republic of Korea
- ⁶⁰ Institute for Gravitational and Subatomic Physics (GRASP), Utrecht University/Nikhef, Utrecht, Netherlands
- ⁶¹ Institute of Experimental Physics, Slovak Academy of Sciences, Košice, Slovak Republic
- ⁶² Institute of Physics, Homi Bhabha National Institute, Bhubaneswar, India
- ⁶³ Institute of Physics of the Czech Academy of Sciences, Prague, Czech Republic
- ⁶⁴ Institute of Space Science (ISS), Bucharest, Romania
- ⁶⁵ Institut für Kernphysik, Johann Wolfgang Goethe-Universität Frankfurt, Frankfurt, Germany
- ⁶⁶ Instituto de Ciencias Nucleares, Universidad Nacional Autónoma de México, Mexico City, Mexico
- ⁶⁷ Instituto de Física, Universidade Federal do Rio Grande do Sul (UFRGS), Porto Alegre, Brazil
- ⁶⁸ Instituto de Física, Universidad Nacional Autónoma de México, Mexico City, Mexico
- ⁶⁹ iThemba LABS, National Research Foundation, Somerset West, South Africa
- ⁷⁰ Jeonbuk National University, Jeonju, Republic of Korea
- ⁷¹ Johann-Wolfgang-Goethe Universität Frankfurt Institut für Informatik, Fachbereich Informatik und Mathematik, Frankfurt, Germany
- ⁷² Korea Institute of Science and Technology Information, Daejeon, Republic of Korea
- ⁷³ KTO Karatay University, Konya, Turkey
- ⁷⁴ Laboratoire de Physique Subatomique et de Cosmologie, Université Grenoble-Alpes, CNRS-IN2P3, Grenoble, France
- ⁷⁵ Lawrence Berkeley National Laboratory, Berkeley, California, United States
- ⁷⁶ Lund University Department of Physics, Division of Particle Physics, Lund, Sweden
- ⁷⁷ Nagasaki Institute of Applied Science, Nagasaki, Japan
- ⁷⁸ Nara Women's University (NWU), Nara, Japan
- ⁷⁹ National and Kapodistrian University of Athens, School of Science, Department of Physics, Athens, Greece
- ⁸⁰ National Centre for Nuclear Research, Warsaw, Poland
- ⁸¹ National Institute of Science Education and Research, Homi Bhabha National Institute, Jatni, India
- ⁸² National Nuclear Research Center, Baku, Azerbaijan
- ⁸³ National Research and Innovation Agency - BRIN, Jakarta, Indonesia
- ⁸⁴ Niels Bohr Institute, University of Copenhagen, Copenhagen, Denmark
- ⁸⁵ Nikhef, National institute for subatomic physics, Amsterdam, Netherlands
- ⁸⁶ Nuclear Physics Group, STFC Daresbury Laboratory, Daresbury, United Kingdom

- 87 Nuclear Physics Institute of the Czech Academy of Sciences, Husinec-Řež, Czech Republic
- 88 Oak Ridge National Laboratory, Oak Ridge, Tennessee, United States
- 89 Ohio State University, Columbus, Ohio, United States
- 90 Physics department, Faculty of science, University of Zagreb, Zagreb, Croatia
- 91 Physics Department, Panjab University, Chandigarh, India
- 92 Physics Department, University of Jammu, Jammu, India
- 93 Physics Program and International Institute for Sustainability with Knotted Chiral Meta Matter (SKCM2), Hiroshima University, Hiroshima, Japan
- 94 Physikalisches Institut, Eberhard-Karls-Universität Tübingen, Tübingen, Germany
- 95 Physikalisches Institut, Ruprecht-Karls-Universität Heidelberg, Heidelberg, Germany
- 96 Physik Department, Technische Universität München, Munich, Germany
- 97 Politecnico di Bari and Sezione INFN, Bari, Italy
- 98 Research Division and ExtreMe Matter Institute EMMI, GSI Helmholtzzentrum für Schwerionenforschung GmbH, Darmstadt, Germany
- 99 Saga University, Saga, Japan
- 100 Saha Institute of Nuclear Physics, Homi Bhabha National Institute, Kolkata, India
- 101 School of Physics and Astronomy, University of Birmingham, Birmingham, United Kingdom
- 102 Sección Física, Departamento de Ciencias, Pontificia Universidad Católica del Perú, Lima, Peru
- 103 Stefan Meyer Institut für Subatomare Physik (SMI), Vienna, Austria
- 104 SUBATECH, IMT Atlantique, Nantes Université, CNRS-IN2P3, Nantes, France
- 105 Sungkyunkwan University, Suwon City, Republic of Korea
- 106 Suranaree University of Technology, Nakhon Ratchasima, Thailand
- 107 Technical University of Košice, Košice, Slovak Republic
- 108 The Henryk Niewodniczanski Institute of Nuclear Physics, Polish Academy of Sciences, Cracow, Poland
- 109 The University of Texas at Austin, Austin, Texas, United States
- 110 Universidad Autónoma de Sinaloa, Culiacán, Mexico
- 111 Universidade de São Paulo (USP), São Paulo, Brazil
- 112 Universidade Estadual de Campinas (UNICAMP), Campinas, Brazil
- 113 Universidade Federal do ABC, Santo Andre, Brazil
- 114 Universitatea Nationala de Stiinta si Tehnologie Politehnica Bucuresti, Bucharest, Romania
- 115 University of Cape Town, Cape Town, South Africa
- 116 University of Derby, Derby, United Kingdom
- 117 University of Houston, Houston, Texas, United States
- 118 University of Jyväskylä, Jyväskylä, Finland
- 119 University of Kansas, Lawrence, Kansas, United States
- 120 University of Liverpool, Liverpool, United Kingdom
- 121 University of Science and Technology of China, Hefei, China
- 122 University of South-Eastern Norway, Kongsberg, Norway
- 123 University of Tennessee, Knoxville, Tennessee, United States
- 124 University of the Witwatersrand, Johannesburg, South Africa
- 125 University of Tokyo, Tokyo, Japan
- 126 University of Tsukuba, Tsukuba, Japan
- 127 Universität Münster, Institut für Kernphysik, Münster, Germany
- 128 Université Clermont Auvergne, CNRS/IN2P3, LPC, Clermont-Ferrand, France
- 129 Université de Lyon, CNRS/IN2P3, Institut de Physique des 2 Infinis de Lyon, Lyon, France
- 130 Université de Strasbourg, CNRS, IPHC UMR 7178, F-67000 Strasbourg, France, Strasbourg, France
- 131 Université Paris-Saclay, Centre d'Etudes de Saclay (CEA), IRFU, Département de Physique Nucléaire (DPhN), Saclay, France
- 132 Université Paris-Saclay, CNRS/IN2P3, IJCLab, Orsay, France
- 133 Università degli Studi di Foggia, Foggia, Italy
- 134 Università del Piemonte Orientale, Vercelli, Italy
- 135 Università di Brescia, Brescia, Italy
- 136 Variable Energy Cyclotron Centre, Homi Bhabha National Institute, Kolkata, India
- 137 Warsaw University of Technology, Warsaw, Poland
- 138 Wayne State University, Detroit, Michigan, United States
- 139 Yale University, New Haven, Connecticut, United States

¹⁴⁰ Yonsei University, Seoul, Republic of Korea

¹⁴¹ Zentrum für Technologie und Transfer (ZTT), Worms, Germany

¹⁴² Affiliated with an institute covered by a cooperation agreement with CERN

¹⁴³ Affiliated with an international laboratory covered by a cooperation agreement with CERN.